TRABAJO ESPECIAL DE GRADO

THE EVALUATION OF SEALING PROPERTIES OF MUDSTONE LAYERS FOR SHALLOW GAS ACCUMULATIONS IN THE DUTCH NORTHERN OFFSHORE

TUTORES ACADÉMICOS: Prof. Ricardo Alezones
Prof. Stéfano Lo Russo

TUTOR INDUSTRIAL: Dr. Hanneke Verweij

Presentado ante la Ilustre
Universidad Central de Venezuela
Por el Br. Valeria A. Daza C.
Para optar al Título
de Ingeniero Geólogo

Caracas, 2012

ACKNOWLEDGMENTS

First of all I would like to show my gratitude to the illustrious Universidad Central de Venezuela for all the knowledge and life experience that I have gain from it and for have given me the opportunity to be part of the bilateral agreement with the Politecnico di Torino in which I have continued my education growing as a person and as a professional.

I want to extent my gratitude to my academic tutors: Prof. Ricardo Alezones and Prof. Stefano Lo Russo for all the support and orientation that they have given me during my formation and to my two supervisors at TNO. To my main supervisor Dr. Hanneke Verweij for her constant advices and review of my work and for have given me the opportunity to be involve in this project which is important for my future career. To Dr. Kees Geel for introducing me to Petrel and for his disposition to clarify any doubts that I could have during the project.

In addition I would like to thank to Prof. Peter Fokker for introducing me to the opportunity to do my thesis at TNO, to all my friends and colleagues for their constant support during the last 6 months and above all to my family which unconditional love and guidance made me the person that I am today.

Daza C. Valeria A.

THE EVALUATION OF SEALING PROPERTIES OF MUDSTONE LAYERS FOR SHALLOW GAS ACCUMULATIONS IN THE DUTCH NORTHERN OFFSHORE

Tutores Académico: Prof. Ricardo Alezones y Prof. Stéfano Lo Russo. Tutor Industrial: Dr. Hanneke Verweij, Tesis. Caracas, U.C.V. Facultad de Ingeniería. Escuela de Geología, Minas y Geofísica. Año 2012, p78.

Palabras claves: sealing capacity, grain size distribution, mudstone layers.

Las capas de lodolita juegan un papel importante en la exploración de hidrocarburos ya que pueden actuar como roca sello en los sistemas petroleros. La presente tesis de grado es parte de un proyecto llevado a cabo por la compañía TNO en el cual se estudian las acumulaciones someras de gas en depósitos del Plioceno – Pleistoceno en la costa afuera de los Países Bajos.

El principal objetivo del presente estudio es evaluar las propiedades capilares de las lodolitas como rocas sello en tres bloques de la costa afuera holandesa. Objetivos secundarios incluyen el análisis de la relación entre su capacidad como roca sello, la profundidad y su posición estratigráfica en el Delta Eridanos.

Fue desarrollado y aplicado un enfoque sistemático para evaluar la capacidad de retención de hidrocarburos que tienen las capas de lodolita basado en el análisis del tamaño de grano y en los datos de presión disponibles. A partir de las distribuciones del tamaño de grano fue construida una base de datos con las principales propiedades como porosidad y permeabilidad. Para finalizar esta base de datos fue usada para calcular la capacidad de sello de cada una de las capas que a su vez fue comparada con las columnas de hidrocarburos calculadas usando los datos de presión.

Los posibles yacimientos de gas fueron encontrados en específicas unidades sismo-estratigráficas. La comparación entre las columnas de gas calculadas usando los datos de presión con las obtenidas a través del análisis del tamaño de grano muestran una buena concordancia en la mayoría de los casos. Por lo tanto el enfoque desarrollado usando el análisis de tamaño de grano puede ser considerado como una herramienta útil para estimar las propiedades de las capas de lodolita y su capacidad como rocas sello.

CONTENTS

LIST OF FIGURES

LIST OF TABLES

LIST OF SYMBOLS

Pc	*Capillary pressure*
Pce	*Capillary entry pressure*
γ	*Interfacial tension*
β	*Wettability*
rr	*Reservoir pore throat radius*
rs = r	*Seal pore throat radius*
Pbouy	*Hydrocarbon buoyancy pressure*
ΔU	*Overpressure*
ρw	*Water density*
ρg	*Gas density*
g	*Gravity*
Pw	*Water pressure*
Pg	*Gas pressure*
Pp	*Pore pressure*
Ts	*Tensile strength of the rock*
h	*Hydrocarbon column*
σ3	*Minimum compressive stress*
k	*Permeability*
θ	*Porosity*
d	*Equivalent grain size diameter*
d10	*Critical grain size diameter*
σv	*Vertical stress*
σ'v	*Vertical effective stress*
T	*Temperature*

CHAPTER I

INTRODUCTION

1.1. PROJECT PRESENTATION

The shallow gas project is a joint industry project aiming to predict target areas for shallow gas that involves the characterization of different interrelated aspects of the shallow gas system.

The shallow gas accumulations may represent a valuable additional hydrocarbon resource, especially if is located near existing infrastructures. Shallow gas production in the Dutch offshore is still limited due to a lack of insight in the shallow gas system especially with respect to the relation between anatomy of the Eridanos delta and the charging - trapping conditions (Schroot & Schüttenhelm, 2003).

This study is focused in a part of the ongoing Shallow gas project; its purpose is to evaluate the sealing properties and continuity of mudstones layers in the A, B and F blocks of the Dutch northern offshore specifically in the wells A12-03, A17-01, A18-02, B10-03, B13-03, B13-04, B16-01, B17-05, B17-06, F01-01, F02-06 and F12-03

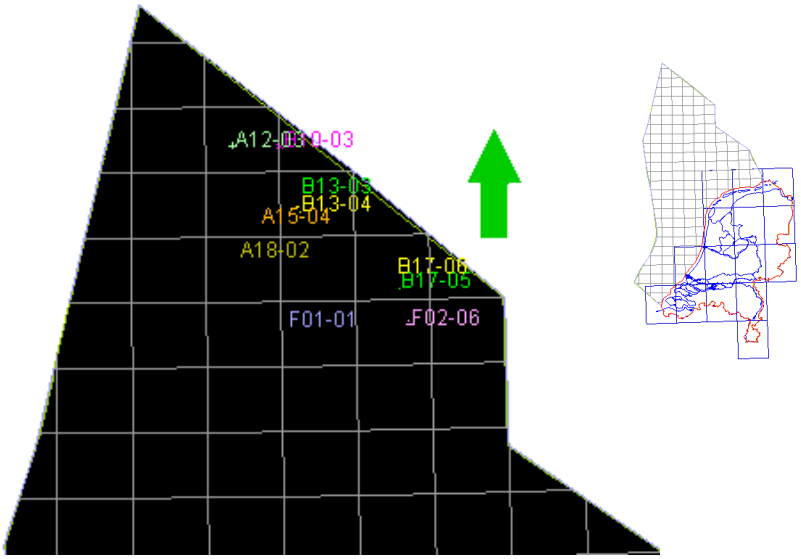

Figure 1-1. Well position in part of the offshore Netherlands, Petrel.

For the present study, shallow gas can be defined as gas in unconsolidated clastic sediments which are above the Mid-Miocene unconformity (1000 – 1500m depth). It predominantly occurs in shallow marine to continental deposits of the Plio – Pleistocene Eridanos Delta (Upper North Sea Group)(Schroot & Schüttenhelm, 2003). This delta was fed by an ancient fluvio-deltaic system that prograded through Northwestern Europe due to simultaneous uplift of the Fennoscandinavian Shield and accelerated subsidence of the North Sea Basin; the dimensions of its drainage area and the thickness of the deltaic deposits make it one of the largest and complex deltas in the world(Verweij, et al., 2012).

In general, deltaic depositional systems respond sensitively to sea level change and climate variability. The deposition of the Eridanos delta sediments occurred under the influence of charging climatic conditions; from the Pleistocene onwards, more frequent sea-level and climate changes disrupted the system, entering glacial cycles. As a result, the shoreline-shelf system formed stacked sequences that reflect changing interrelations between accommodation (sea level), climate conditions and sediment supply.(Donders, et al.)

Shallow gas in marine sediments are mostly composed of methane, but can also include carbon dioxide, hydrogen sulphide and ethane (Schroot & Schüttenhelm, 2003). The origin of the shallow gas may be from deep subsurface thermogenic sources or biogenic sources in shallower strata and it is either structurally trapped in anticlines associated with rising salt domes or occurs in stratigraphic or depositional traps. Biogenic methane was originally believed to be produced only within the top few meters of seabed sediment, but now there is evidence for bacterial activity even at a few hundred meters below seabed. With rapid sedimentation, bacterial gas accumulations may be buried to depths far below those at which the gas was biogenically produced. Thermogenic methane is produced from organic precursors at high temperatures and high pressures, and consequently is generated at depths greater than 1000m. Such gas may, however, migrate towards the surface and accumulate in shallow sediment layers. It is not easy to determine whether methane was biogenically or thermogenically formed (Schroot & Schüttenhelm, 2003)

The shallow fields and prospects in the area of interest often consists of multiple stacked reservoirs above the salt domes, forming salt-induced, low relief anticlines trapping the gas; this structures normally occurs at depths ranging from 300 to 800m.(Van den Boogaard & Hoetz, 2012).

There have been identified gas chimneys, acoustic turbidity and blanking, pockmarks and stacked bright spots that indicate highly dynamics systems with ongoing and/or recent migration of shallow gas. At present, migration and charging of biogenic gas generated in the Eridanos delta takes place under normal to close to normal pore pressure conditions. Hence the migration will involve flow of methane dissolved in groundwater and buoyancy-driven separate phase migration of gas towards conventional stratigraphic and structural traps (Schroot & Schüttenhelm, 2003).

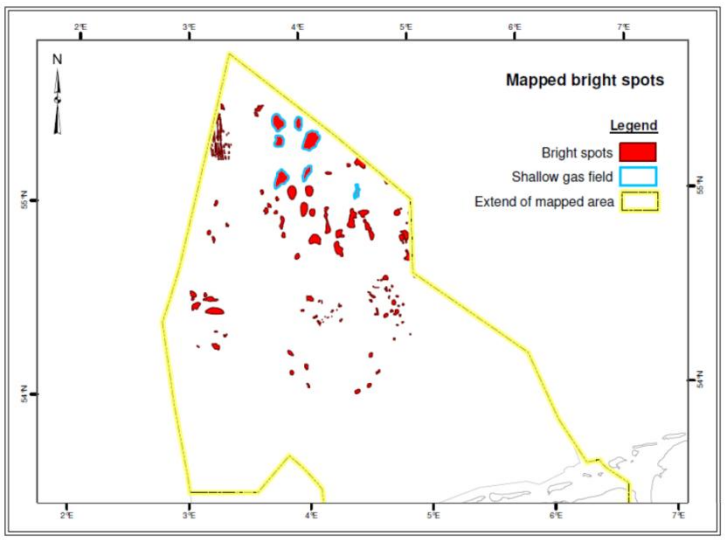

Figure 1-2. Extent of the bright spot mapping performed by TNO (2009)

1.2. OBJECTIVES

The main purpose of the present study is to evaluate the sealing capacity of the mudrocks layers in shallow gas reservoirs and its relation with depths and stratigraphic position. From this evaluation is possible to estimate the hydrocarbon columns that the seals can retain and understand the continuity of the sealing properties in the stratigraphic sequences.

The first part of the study includes:

- Relate the location of the gas bearing layers and the sealing layers in the wells A12-03, A17-01, A18-02, B10-03, B13-03, B13-04, B16-01, B17-05, B17-06, F01-01, F02-06 and F12-03 with the seismic stratigraphic sequences.

From the grain-size distribution of the sealing layers, the aim is to :

- Make a lithological description and classification of the mudrocks from the grain-size distribution.
- Create a database with the relevant properties of the sealing layers located among 12 wells of the blocks A, B and F in the Dutch northern offshore for shallow gas reservoirs.

- Correlate the changes in the sealing properties with depths, well location and stratigraphic position.
- Compare and relate the hydrocarbon columns obtained by the grain-size with the obtained by pressure data.
- Relate sealing layers properties with the depositional environments.

1.3. LITERATURE REVIEW

1.3.1. Seals

A seal rock (cap-rock), can be defined as a formation with extremely low porosity and permeability overlying an oil or gas reservoir and which constitutes the barrier against the volume flow of hydrocarbons into the upper layers (Li, Dong, Li, Huang, & Qing, 2005); it is one of the essential elements of petroleum systems together with the source and the reservoir rock.

Seal Classification

Watts (1987), proposed a general classification of the seal behavior dividing them in *membrane* and *hydraulic seals*. The former refers to those controlled by capillary properties of the interconnected pore throats, while in the hydraulic seals the capillary pressure is so high that the seal preferentially fails by fracturing (Darby, 2002).

There is another seal classification scheme proposed by (Boult, Lanzilli, Michaelsen, McKirdy, & Ryan, 1998), which includes all aspects of entrapment and migration/flow through seals. In base to this classification, there are effectively three main types of seal which control the entrapment and production of hydrocarbons:

- *Pressure seals* is where the buoyant fluid is held back by the wall of water flowing downwards through the pores due to a pressure potential which can be considered to be an equivalent column of water or "head"; It enhances the HC sealing potential and favors downwards migration. Normally occurs in ***undercompacted shales*** *(sand-shale dominated contexts / tertiary basins)* ***Highly strained shaly seals (****Sand shale offshore compressive domains/in onshore Foothills) and* ***Shaly seals with high OM content / COALS*** *(During peak HC generation)* (Grauls, 2011). These seals are total barriers to the flow of both hydrocarbons and water and are normally of regional extend. In theory, due to the low permeability, they may temporarily exist as confined barriers to flow during production (Boult, Lanzilli, Michaelsen, McKirdy, & Ryan, 1998)

- *Permeability seals* are total barriers to neither hydrocarbons nor water. They are very common in production situations where they may either prevent efficient hydrocarbons extraction or enhance it if the production strategy is optimized. Permeability seals are only effective in entrapment situations during active migration when hydrocarbons will 'back up' behind them or, for a limited time, as hydrocarbons leak away after a capillary seal has been breached. (Boult, Lanzilli, Michaelsen, McKirdy, & Ryan, 1998)

-*Capillary seals* are total barriers only to the flow of separate-phase hydrocarbons. They can be effective during entrapment or production. Once breached, capillary seals may then act as permeability barriers due to their finer grain size. (Boult, Lanzilli, Michaelsen, McKirdy, & Ryan, 1998). Capillary seals rely on the balance between opposing forces of gravity (buoyancy) and capillarity in order to seal. The migrating hydrocarbons will eventually encounter the overlying top seal rock and spread out along the sealing boundary. A capillary seal acts as a perfect seal for those hydrocarbons until the hydrocarbon buoyancy pressure, exerted by the increasing column, exceeds the top seal capillary entry pressure, at which point leakage will take place by permeable two phase flow.(Ingram, Urai, & Naylor, 1997).

Sealing Mechanisms

Several authors (Concoran & Doré, 2002) have mentioned four generic mechanisms by which top seals leak: tectonic breaching, capillary leakage, hydraulic leakage and molecular transport.

- **Capillary Sealing**

Both hydrocarbons and water may migrate through sealing rocks from a pressure compartment via the pore network of the cap rock. However, the processes that control hydrocarbon retention below a seal are different from those that control the water movement through reservoirs and cap rocks. Water flux is controlled by the intrinsic permeability and hydraulic gradient in rocks according to Darcy's law; water will therefore leak in all directions toward lower hydraulic heads (overpressures). Reservoired hydrocarbons will flow through the pore network of a water-wet seal only if the capillary entry pressure (Pce) has been overcome by the buoyancy of the underlying hydrocarbons (Berg, 1975)

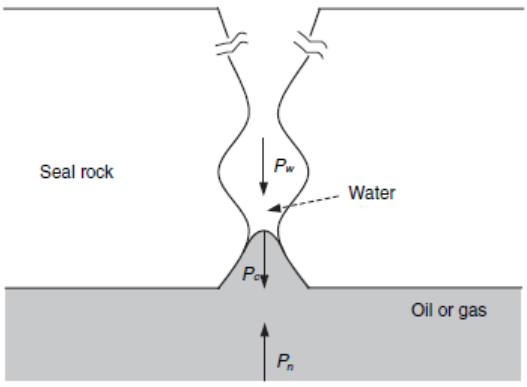

Figure 1-3. Schematic of capillary sealing mechanism in a pore throat of seal rock (Li, Dong, Li, Huang, & Qing, 2005).

The Figure 1-3 shows a pore throat and a curved interface between the wetting (water) and nonwetting phases (oil or gas) in a seal rock, where Pn is the pressure in the non-wetting phase, Pw is the pressure in the wetting phase, and Pc is the capillary pressure across the nonwetting/wetting meniscus in a porethroat.

The capillary pressure prevents the penetration of the non-wetting fluid into the seal rock through slow Darcy flow. (Li, Dong, Li, Huang, & Qing, 2005); it depends of the difference in size between pore throats in the reservoir and the seal, the interfacial tension between hydrocarbon and water and the and the angle of contact of the hydrocarbon-water interface against the adjacent rock grains (wettability).

$$Pc = 2\gamma \left(\frac{1}{rs} - \frac{1}{rr}\right) cos\beta \qquad \textbf{(1)}$$

As the pore throat radius of the reservoir is too higher in comparison with the pore throat radius of the seal, the term $(\frac{1}{rr})$ can be considered as negligible. In practice if the seal is water wet when failure occurs, then the contact angle can also be assume to be 0 so cosβ becomes unity.

$$Pc = 2\gamma/r \qquad \textbf{(2)}$$

The capillary fluid flow properties of the rock that govern sealing behavior include porosity, permeability and capillary entry pressure. These properties are influenced by chemistry (including depositional composition and subsequent diagenetic modifications), and the effective stress acting on the rock which is a function of depth and fluid pressure. (Darby, 2002). There is possible to find in the literature different names for the pressure that have to be overcome in order to start the hydrocarbon leakage from a seal: Capillary entry pressure(Ingram, Urai, & Naylor, 1997), Threshold capillary pressure (Aplin & Larter, Fluid flow, pore pressure, wettability, and leakage in mudstone cap rocks., 2005) and Breakthrough pressure (Li, Dong, Li, Huang, & Qing, 2005).

The concept of entry (displacement) pressures (Berg, 1975) has been used for many years to describe the sealing potential of traps. The use of entry pressures results in a static assessment of cap rocks sealing potential, which means that the oil and/or gas column that can be supported by a cap rock is considered to be constant as long as the properties of the cap rock do not change. The former changes can occur during geological time as result of burial and associated compaction and diagenesis, but not as a result of the hydrocarbon flow itself; **therefore, according to this assessment, leakage does not change the sealing potential of a cap rock.** Once the entry pressure of a cap rock have been exceeded by a hydrocarbon column, the trap will be unable to support any additional column and all hydrocarbons subsequently supplied to the trap will leak out of it.(Sylta, 2005)

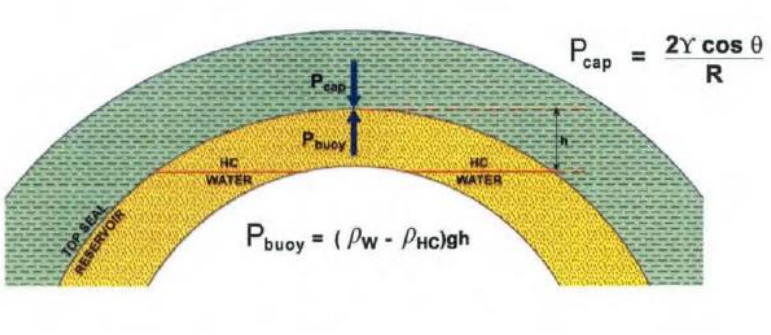

Figure 1-4. Capillary leakage scheme (Concoran & Doré, 2002)

The Figure 1-4 shows the pressures acting in the boundary of the reservoir and the top seal, being h the maximum column of hydrocarbon above the water contact that the seal can hold.

There is possible to find in the literature different names for the pressure that have to be overcome in order to start the hydrocarbon leakage from a seal: Capillary entry pressure, Threshold capillary pressure and Breakthrough pressure.

Seal Capacity

The seal capacity is the height of the hydrocarbon column that the seal may retain prior to leaking; it is a function of the pore throat size distribution along largest interconnected pore throat path through the seal, the density of the hydrocarbons, the density of the formation water, the formation water pressure and other factors. (Barboza, Alway, Akpulat, Esch, Hicks, & Gerdes, 2009)

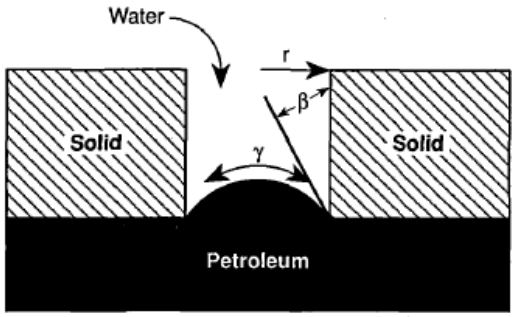

Figure 1-5 Definition of terms referred to the capillary resistance calculations. (Clayton & Hay, 1994)

In the Figure 1-5 is possible to observe in the pore throat the water-petroleum contact, the wettability and the interfacial tension acting on it.

For failure to occur the upward buoyancy pressure plus any excess overpressure ` relative to the seal (ΔU) must exceed the capillary resistance:

$$Pbuoy + \Delta U > Pc \qquad (3)$$

$$(\rho w - \rho hc)gh + \Delta U > Pc \qquad (4)$$

This equation can then be rearranged to calculate the maximum petroleum column height which a seal can hold back

$$h = \frac{2\gamma cos\beta}{r(\rho w - \rho hc)g} - \frac{\Delta U}{(\rho w - \rho hc)g} \qquad (5)$$

In essence, the first part of the right hand side of the equation gives the normal column height which can be expected, and the second part gives a correction for excess overpressure in the reservoir. There are also two additional conclusions that are possible to derived from this equation:

- If the migration path through the seal becomes oil-wet or gas-wet then the $2\gamma cos\beta$ term reduces, ultimately reaching zero. In other words, the resistance to flow approaches zero and the seal will continue to leak even after the column height drops below the critical value.
- There is not term for the thickness of the seal. Very thin seals if they are continuous, are just as efficient as thick seals.(Clayton & Hay, 1994)

Lithology , uniformity of stratigraphy and thickness as is possible to observe in Figure 1-6, are factors which can influence seal capacity; however, the fundamental rock properties which control seal performance are the capillary entry pressure of the seal and the ductility of the seal rock which is a function of pressure, temperature and lithology. (Concoran & Doré, 2002). Thicker seals may be better equipped to resist breaching by faults, but will not retain grater columns by capillary resistance.(Ingram, Urai, & Naylor, 1997)

The pore throat radius is the most important variable in the seal capacity calculation and it is also the most difficult to estimate. Hydrocarbons entering in the seal will not flow through all of the pores in the rock but will seek the largest interconnected pores and take the easiest route. The capillary resistance force will therefore be a function of the smallest pore throat encountered on this interconnected pore network; it will be neither the smallest pore throats in the rock (Clayton & Hay, 1994)

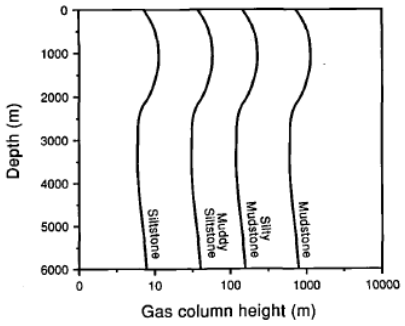

Figure 1-6 Effect of different lithologies on seal capacity for dry methane. (Clayton & Hay, 1994)

Mudstones are the most abundant sedimentary rocks and can act as sources, seals or unconventional reservoirs in petroleum systems; usually comprise sediments which size diameter is less than 62,5 μm and in general, due to their low permeability and as a consequence, high capillary entry pressure, behave as seals and as flow baffles in conventional reservoirs. Their low permeability is critical to the retention of fluid in sedimentary basins and thus the occurrence of overpressure; however muds allow the transmission of substantial volumes of fluid on geological time scales.(A.C & Macquaker, 2011).

Compaction, permeability and seal capacity are some of the linked properties of mudstone cap rocks that must be described in two-phase fluid flow models of petroleum systems (Aplin & Larter, 2005).

Rocks that undergo stress-sensitive compaction will not compact further in the hypothetical case when the pressure compartment is completely sealed off. At this stage, subsidence may proceed, but because the effective stress is not further increased, the pore pressure stay constant.(Hermanrud, Nordgard, & Teige, 2005)

Mudstone compaction is commonly described as a purely mechanical process in which porosity is lost in response to increasing effective stress. Because compaction represents a volumetric reduction of porosity, relationships

between porosity and effective stress should strictly be couched in terms of mean effective stress but usually is related to vertical effective stress instead of the mean one. (Aplin & Larter, 2005)

The porosity-effective stress equation used quantitatively as a means of describing mudstone compaction and evaluating pore pressure from mudstone porosity data requires the numerical values of the coefficients β and e100. (Aplin & Yang, 2004) derived from soil mechanics literature the relation between compression coefficients and clay content considering clay as particles with a diameter less than 2μm.

The previous relationships were constructed using data from 21 North Sea wells, one well from the Gulf of Mexico and data for both natural and remolded muds compacted to low levels of effective stress; they show that the compression coefficients are strongly dependent on clay content and if one can determine the clay content of a fine-grained clastic sediment, the mechanical compaction curve (relationship between void ratio and effective stress) can be define accurately. (Aplin & Larter, Fluid flow, pore pressure, wettability, and leakage in mudstone cap rocks., 2005).

There exist also another equations that correlates the clay content with the compaction coefficients derived from Skempton (1970) and Burland (1990) datasets; they are based on a relatively small number of data points for sediments that have been generally subjected to stress level less than 5MPa, corresponding to only a few hundred meters burial depth (Aplin & Yang, 2004)

The largest interconnected pore throat diameter is the critical factor with respect to the capillary entry pressure of the mudstones; in tight mudstones, the risk of capillary failure is very low as the capillary entry pressure commonly exceeds the buoyancy force of any potential hydrocarbon column. In this case, the top seal retention capacity of the Mudrock is a function of the ductility of the mudstone and the potential for the formation of dilatants fractures (Concoran & Doré, 2002).

Other relevant aspect to consider is the fact that Cap-rock units can manifest vertical and lateral heterogeneities. Internal lithostratigraphy of the unit can vary with mudrocks interbedded by leaky strata such as sandstones; this can result in multimodal porethroat diameter distributions within the cap-rock interval. (Concoran & Doré, 2002)

Capillary leak can occur predominantly in offshore shallow buried shaly seals (low compacted seals), waste zones, high sand content shaly seals, fractured seals (shales, carbonates, etc) and in low pressured domains. For the contrary is unlike that it occurs in deeply buried shales (highly compacted seals), tight unfractured carbonates, diagenetic seals and evaporitic seals which are more disposed to fracture. (Grauls, 2011)

- ***Tectonic breaching*** where deformation of a cap rock occurs post-emplacement of hydrocarbons there is an increased risk of tectonic breaching and cap-rock leakage.

- ***Molecular transport***

Diffusion is a continual process in sedimentary basins; the diffusive transport mechanism primarily pertains to the migration of natural gas accumulations in certain circumstances and has little relevance for oil migration due to the increased size of molecules relative to shale pore throat dimensions. The diffusion model proposed by Leythaeuser et al. (1982) suggests that the evolution and preservation of natural gas accumulations is dependent upon the ratio of gas supply to the trap and gas losses through the cap rock. (Concoran & Doré, 2002)

- Hydraulic leakage – Fracture Failure

Where the capillary entry pressure to a cap-rock (evaporate or super tight shale) are so high that capillary failure is unlikely, hydraulic leakage may occur through brittle top-seals due to generation of new tension failures (hydrofractures), shear fractures or the dilation of pre-exiting fault planes. Hydraulic fracturing can occur independent of tectonic breaching and results from changes in effective stress conditions in the cap-rock (Concoran & Doré, 2002)

Failure of seals by fracturing will occur when the pore fluid pressure induced by overpressuring and petroleum buoyancy exceeds the local rock strength and the tensile strength holding the rock together; therefore the evaluation of the seal integrity of a cap rock is a function of its resistance to hydraulic fracturing (pore pressure / minimum stress)(Clayton & Hay, 1994)

$$Pp > S + Ts \qquad (6)$$

Mudrocks are very weak under subsurface conditions so is possible to ignore the tensile strength; it is often more convenient to think in terms of the effective stress σ, which is the difference between the total stress pushing the rock together and the pore fluid pressure pushing it apart again:

$$\sigma = (S - Pp) \qquad (7)$$

The rock will fracture when the effective stress becomes zero; fractures will form perpendicular to the minimum effective stress (σ3) direction consequently as normally σ3 is horizontal, vertical fractures will form. Then, fracturing and faulting are initiated when the stress state is such that the failure condition for the rock is met.

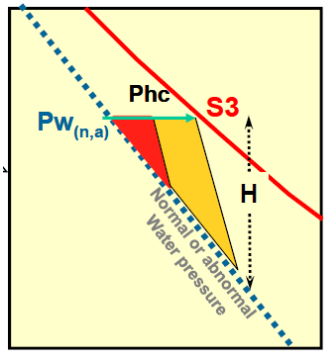

Figure 1-7 Fracture failure (Grauls, 2011)

1.3.2. Grain-size classification systems

Traditionally, it has been defined four size fractions that include gravel, sand, silt, and clay, to classify these sediments based on ratios of the various proportions of the fractions. According to the Wentworth grade scale gravel-sized particles have a nominal diameter of 2 mm, sand-sized particles have nominal diameters from <2 mm to >62.5 µm, silt-sized particles have nominal diameters from <62.5 µm to >4 µm and clay is < 4 µm; there also exist others classifications like the one used by Aplin (2004) in which clay particles are consider < 2 µm.

Several classification schemes have been adopted to describe the approximate relationship between the size fractions; the systems more used are the ones of Shepard (1954) or Folk (1954, 1974). The original scheme devised by Shepard (1954) utilized a single ternary diagram with sand, silt, and clay in the corners to graphically show the relative proportions among these three grades within a sample. To classify sediment samples, Shepard (1954) divided a ternary diagram into ten classes; for example, Shepard's "Clays" contain at least 75% clay-sized particles. "Silty Sands" and "Sandy Silts" contain no more than 20% clay-sized particles, and "Sand-Silt-Clays" contain at least 20% of each of the three components. (Shepard, 1954)

Although this scheme does not allow for sediments with significant amounts of gravel, Schlee in 1973 modified it, adding a second ternary diagram to account for the gravel fraction.

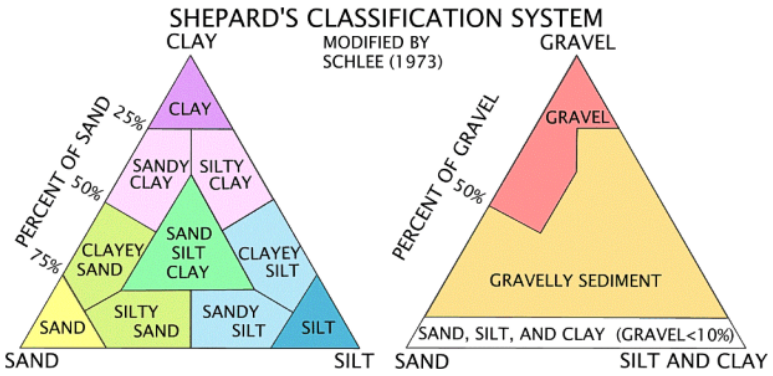

Figure 1-8 Shepard's classification system (Survey)

The system devised by Folk (1954, 1974) is also based on two triangular diagrams, but it has 21 major categories, and uses the term mud (defined as silt plus clay). The patterns within the triangles of both systems differ, as does the emphasis placed on gravel. For example, in the system described by Shepard, gravelly sediments have more than 10 percent gravel; in Folk's system, slightly gravelly sediments have as little as 0.01 percent gravel.

Folk's classification scheme stresses gravel because its concentration is a function of the highest current velocity at the time of deposition, together with the maximum grain size of the detritus that is available; Shepard's classification scheme emphasizes the ratios of sand, silt, and clay because they reflect sorting and reworking .

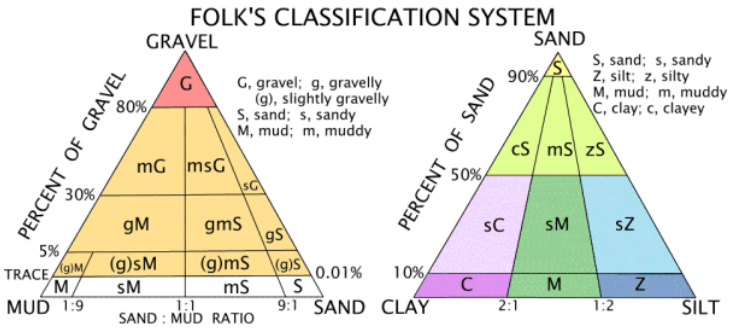

Figure 1-9 Folk's classification system (Survey)

CHAPTER II.

METHODOLOGY

In order to calculate the Mudstones sealing capacity of shallow gas accumulations in the Netherlands offshore were made the following assumptions:

- The mudstones seals are capillary seals or membrane seals which are controlled by capillary properties of interconnected pore throats. The leakage mechanism is capillary leakage that occurs when the upwards buoyancy pressure of a hydrocarbon column exceed the P_{cap} of the top-seal**.**
- The assessment of the cap-rock sealing potential is static; this means that the oil and/or gas column that can be supported by a cap rock is considered to be constant as long as the properties of the cap rock do not change. In this sense, the leakage does not change the sealing potential of a cap rock; once the entry pressures of the cap rock have been exceeded by an hydrocarbon column, the trap will be unable to support any additional column and all hydrocarbons subsequently supplied to the trap will leak out of it **.**
- The Capillary pressure of the seal (gas-entry pressure) is not a function of the fluid saturations or fluid flux into the seal.
- The gas-water contact angle is zero (wettability); this implies that the wetting phase (brine) completely wets the solid surfaces and the wettability does not change with time**.**

2.4. LITHOLOGICAL CHARACTERIZATION

In order to characterize the lithology of the samples from the grain-size distribution were used two main classifications:

2.4.1. Clay Particles < 2µm

Is the classification used in soil mechanics in which the clay size is defined as particles with diameter less to 2µm, normally using the pipette method to obtain the grain size distribution. The most common subdivision of soil granulometry into classes is the fine earth, for particles ranging from 0 to 2mm (2000µm), and coarse particles, for particles bigger than 2mm(Moeys, 2012).

Fine earth is generally divided into 3 particle size classes: clay (fine particles), silt (medium size particles) and sand (coarser particles in the fine earth). All soil scientists use the range 0-2µm for clay; so silt lower limit is also always 2µm. But the convention for silt / sand particle size limit varies from country to country. (Moeys, 2012)

In this study is used the silt classification as particles which size is between 2-63µm as is the conventional classification used in the Netherlands; therefore the sand particle range used is 63-2000µm.

As the grain-size distribution was measure with the laser diffraction technique, were chosen the particles < 8µm as the equivalent to < 2µm clay particles based in the classification proposed by (Konert & Vandenberghe, 1997); remaining the silt and sand particles size as 8 - 63µm and 63 - 2000µm respectively.

The Shepard's classification system was chosen to describe the approximate relationship between the size fraction due that it reflects the sorting and reworking for which have been through the sediments. The former diagram was made by the **Triangular diagram plotting spreadsheet (TRI-PLOT)** created by David Graham (Loughborough University) and and Nicholas Midgley (Liverpool John Moores University).

As the sorting can be attribute in some cases to specific depositional environments; this classification was used to describe and characterize the possible environments in which the mudstones layers were deposited and relate it with the sorting classification based in the standard deviation values obtained by the grain size distributions.

Normally this system is based in the Wentworth classification, typically used by geologist and geomorphologists to describe the size distributions of the sediments, which clay fraction range is < 4μm. Due to the underestimation of the clay content in the laser diffraction technique, was defined as previously the clay as particles with size < 8μm.

2.5. TOP-SEAL ASSESSMENT

After characterized lithologically the mudstones layers was used the following scheme to assess the following scheme to assess the Mudstone's layers capacity.

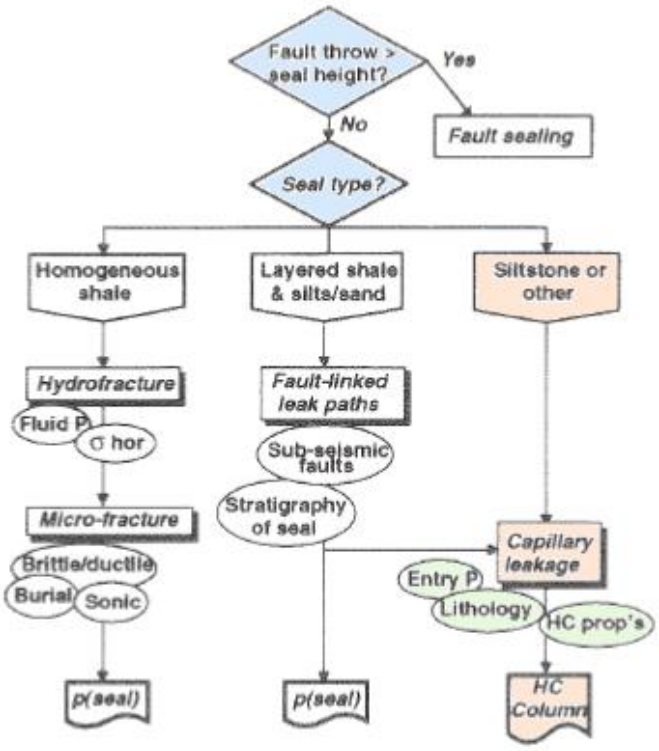

Figure 2-1. Simplified evaluation strategy for top seal assessment.(Ingram, Urai, & Naylor, 1997)

The flow chart begins by determining if faults throws are greater than the top seal thickness. If so, then a fault seal analysis is an additional requirement which is not the case of the present study.

The rectangles represent leakage scenarios and the ellipses indicate data which will contribute to analysis of the scenarios (HC prop's are the hydrocarbon physical properties, including wetting characteristics). (Ingram, Urai, & Naylor, 1997)

Top seals are simplified into three main types: massive shale, layered shale/sand/silt, and massive strata of siltstones and other coarse grained lithologies. Based in the lithological characterization of the mudstones layers, were chose the third path for the top seal assessment in which the hydrocarbon column calculations is based in capillary leakage instead of hydrofracturing.

2.5.1. Assessment of Sealing Capacity by grain size distribution

Key parameters in order to estimate the sealing capacity of mudstones for gas accumulations are the pore throat diameter, the interfacial tension, gas density and permeability.

$$\boldsymbol{h = \frac{2\gamma}{r(\rho w - \rho g)g}} \qquad \textit{(8)}$$

Pore Throat Radius $h = \frac{2\gamma}{r(\rho w - \rho g)g}$

In order to assess the pore throat ratio, as it is not a common parameter among geologists, were measured the grain-size distribution of sealing layers of shallow gas accumulations in the Netherlands offshore. This samples corresponds to the wells A15-04, A18-02, B10-03, B13-03, B13-04, B17-05, B17-06, F01-01 and F12-03 in a range between 339 to 927 m SSTVD

To estimate the pore throat size of the Mudstone layers, first parameter necessary to calculate the sealing capacity, was used the ***Equivalent grain size method*** (Nakayama & Sato, 2002). In this method is assumed that a cap rock consists of equalized grains; the pore-throat can be regarded as a function of grain size and porosity if the geometrical ratio of pore-throat and grain size is considered. Although porosity does not change as grain size changes, it does change according to the packing; for this reason there is a relationship between the ratio

of pore-throat size to grain size (COEF) and porosity according to the theoretical types of packing.

From this method were obtained the following relations:

$$\boldsymbol{COEF} = 1.92(\theta)^2 - 0.0882(\theta) \qquad \textbf{(9)}$$

$$\boldsymbol{r} = \frac{1}{2}(COEF)d \qquad \textbf{(10)}$$

Substituting ***Equation 0-*** (in ***Equation*** ***(***1 is obtained:

$$\boldsymbol{r} = \frac{1}{2}\left(1.92(\theta)^2 - 0.0882(\theta)\right)d \qquad \textbf{(11)}$$

The unknown of this equation in order to obtain the pore throat radius is the porosity; the median and mean grain size diameter were selected as the '*equivalent grain size'* and were obtain from the grain size distribution.

The pore throat radio was also calculated using the following equation:

$$log(dc) = 0.7187 * log\, k + 5.5655 \qquad \textbf{(12)}$$

The former equation was obtained from the Yang and Aplin data sets. The d_{10} data should provide close approximations of the critical pore throat diameters of the samples (d_{10} = dc). The d_{10} data of Yang and Aplin range form10 to 1000nm with the corresponding permeabilities from $5x10^{-7}$ to $3x10^{-3}$ respectively. (Norgard, Hermanrud, & Gunn, 2005).

Porosity $\boldsymbol{r} = \frac{1}{2}\left(1.92(\boldsymbol{\theta})^{\mathbf{2}} - 0.0882(\boldsymbol{\theta})\right)\boldsymbol{d}$

The calculation of porosity was made by the relationship between porosity and effective stress used in Soil Mechanics. Mudstone compaction has commonly been described as a purely mechanical process in which porosity is lost in response to increasing effective stress. In soil mechanics, the relationship between porosity and effective stress is described as:

$$e = e100 - \beta \ln\left(\frac{\sigma' v}{100}\right) \quad \textbf{(13)}$$

$$\sigma' v = \sigma v - Pp \quad \textbf{(14)}$$

$$e = \frac{\theta}{1 - \theta} \quad \textbf{(15)}$$

In order to calculate the compaction coefficients were used the equations proposed by ***Yang and Aplin (2004)*** in the ‘’***Definition and practical application of mudstone porosity-effective stress*** **relationship’’** who derived equations between compression coefficients and clay content from natural mudstones using their own data set ***(Equation 16 and 17)*** and datasets taken from Skempton (1970) and Burland (1990) ***(Equation 18 and 19):***

$$e100 = 0.3024 + 1.6867clay + 1.9505clay^2 \quad \textbf{(16)}$$

$$\beta = 0.0407 + 0.2479clay + 0.3684clay^2 \quad \textbf{(17)}$$

$$e100 = 0.659 + 0.592clay + 2.424clay^2 \quad \textbf{(18)}$$

$$\beta = 0.0686 + 0.0937clay + 0.384clay^2 \quad \textbf{(19)}$$

The vertical effective stress was calculated form the lithostatic gradient derived from RHOB log at the well B18-02 for depths between 400 – 1200m with a R^2 = 0.997

$$\sigma v = 0.0216 * z \quad \textbf{(20)}$$

The formation water pressure (*Pw*) was calculated from fluid pressure gradients derived from measured RFT pressures at 9 wells (A12-03, A15-02, A15-03, A18-02, B10-03, B13-03, B13-04, B16-01, B17-05)

$$Pw = 0.0105 * z \quad \textbf{(21)}$$

Hence:

$$\sigma' v = 0.0111 * z \quad \textbf{(22)}$$

Once obtained the compaction coefficients, using equation (13) is possible to calculate the void ratio *(e)* and therefore the porosity *(ϕ).*

Interfacial tension $h = \frac{2\gamma}{r(\rho w - \rho g)g}$

The interfacial tension variation of the water-gas system with depth, was estimated by a depth – interfacial tension relationship (Norgard, Hermanrud, & Gunn, 2005)

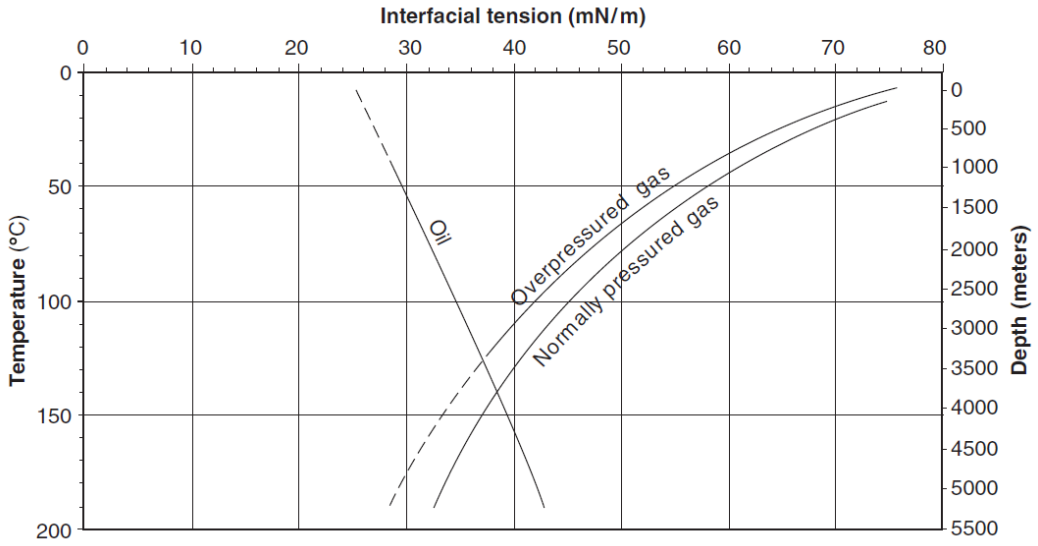

Figure 2-2 Oil and gas interfacial tension calculated from the relationship established by Firoozabadi & Ramey (1998). (Norgard, Hermanrud, & Gunn, 2005)

In order to calculate the interfacial tension for each depth was built a linear relation using the values of interfacial tension at 500m (68mN/m) and 1000m (60,8mN/m) obtained it from the normally pressured gas curve in the figure above.

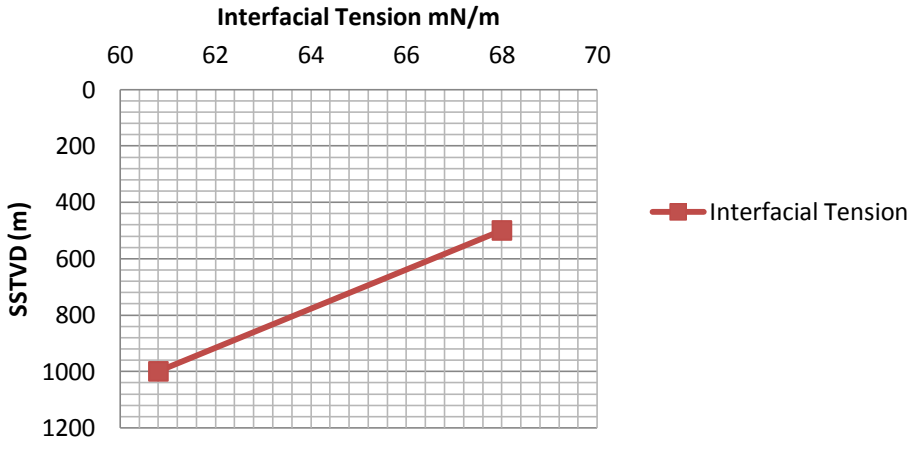

Figure 2-3. Calculated interfacial tension

The equation obtained was:

$$\gamma = \frac{5222.2 - z}{69.44} \qquad \textbf{(23)}$$

In which ***z*** *is the SSTVD in meters and* ***γ*** *the water-gas interfacial tension in mN/m.*

Gas Density $h = \frac{2\gamma}{r(\rho w - \boldsymbol{\rho g})g}$

The gas densities at different depths were calculated from **Material Measurement laboratory** from the **National Institute of Standards and Technology**. (Technology, 2011)

The input data necessary is temperature and pressure which were calculated using the following equations respectively derived from the temperature and pressure gradients respectively:

$$T = 0.030(Z) + 10 \qquad \textbf{(24)}$$

In which T is temperature in ^{o}C *and Z is SSTVD in m.*

$$P = 0.0105\ (Z) + 0.101325 \qquad \textbf{(25)}$$

In which P is pressure in MPa and Z is SSTVD in m.

Water density $h = \frac{2\gamma}{r(\boldsymbol{\rho w} - \rho g)g}$

The water pressure gradient was derived from RFT pressure measurements in the wells A12-03, A15-02, A15-03, A18-02, B10-03, B13-03, B13-04, B16-01 and B17-05.

$$w = 0.0105\ MPa/m$$

$$w = g\rho w \qquad \textbf{(26)}$$

Knowing Ϭw, by the following equation, is possible to calculate the water density:

$$\rho w = \frac{w}{g\ 10^3} \qquad \textbf{(27)}$$

In which ρw is water density in Kg/m^3, Ϭw is water pressure gradient in MPa/m and g is the gravity.

Permeability Calculation

The relation used to calculate the permeability of the sealing layers, was the one proposed by Yang and Aplin (2010) in ***A permeability-porosity relationship for mudstones***. The aim if the authors was to construct a relationship between bedding perpendicular, absolute permeability and porosity for homogeneous, fine-grained clastic sediments.

$$Ln(k) = -69.59 - 26.79clay + 44.07clay^{0.5} + (-53.61 - 80.03clay + 132.78clay^{0.5})e + (86.61 + 81.91clay - 163.61clay^{0.5})e^{0.5} \qquad \textbf{(28)}$$

For a given porosity, mudstone permeability can vary over a range of 2-5 orders of magnitude so the previous equation introduce a quantitative lithology descriptor (clay content) as a constrain in order to reduce this variation for a single value of porosity. By including clay content as a discriminator, an uncertainty of 2-5 orders of magnitude in permeability at a given porosity is reduce to 1 order of magnitude.

2.5.2. Calculation of hydrocarbon columns by pressure data

In order to calculate the hydrocarbon column from pressure data was use equation 29:

$$h = \frac{(Pgas - w * z)}{(\rho w * g - \rho gas * g)} \qquad (29)$$

In the former equation the upper term refers to the overpressure at the depth (z) cause by the gas presence.

The first step to calculate the hydrocarbon columns from pressure data is to identify the measured pressure points corresponding to water and to gas presence; this is made by the compilation of log data (gas peaks and cross-overs of NPHI-RHOB), DHIs from seismic and the pressure data itself.

Water Gradient and density calculation

The water gradient was calculated plotting the RFT pressure measurements in the wells.

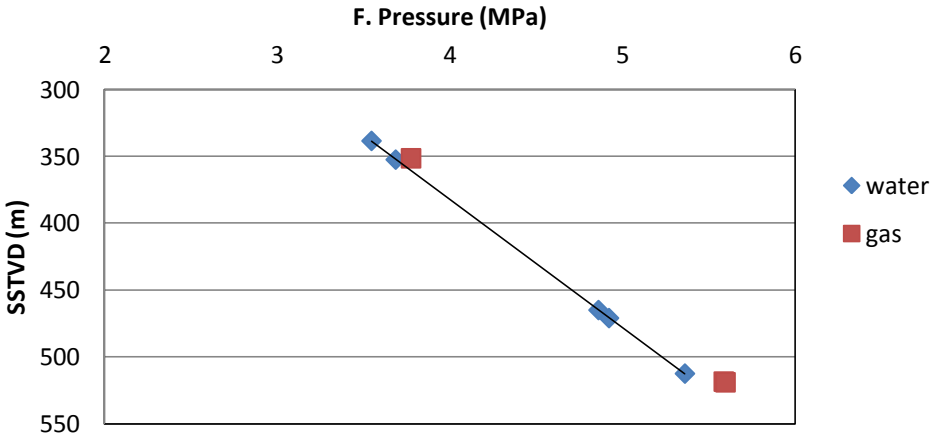

Figure 2-4. Water gradient

As is possible to see in Figure 2-4 was plotted f. pressure vs depth; once identify the water pressure trend were chose two water measurements to calculate the gradient by the following equation:

$$w = \frac{Pwf - Pwi}{Zf - Zi} \qquad \textbf{(30)}$$

Once obtained the water gradient (бw) was possible to obtain the water density in each well by the

$$w = \rho w * g \qquad \textbf{(31)}$$

Gas Density

The gas densities at different depths were calculated from **Material Measurement laboratory** from the **National Institute of Standards and Technology**. (Technology, 2011)

The input data necessary is temperature and pressure; the pressure values were taking directly from the RFT data while the temperatures were calculated using the following equation derived from the temperature gradient:

$$T = 0.030(Z) + 10 \qquad \textbf{(32)}$$

In which T is temperature in ^{o}C and Z is SSTVD in m.

CHAPTER III

RESULTS AND DISSCUSSION

3.1. Gas- bearing layers and seals location

Based in the compilation of log-data and DHIs from seismic were found the gas-bearing layers in 5 principal seismic stratigraphic units:

3.1.1. Seismic stratigraphic units s12 and s13

In the top of the seismic stratigraphic unit s12 there is evidence of bright spots in the wells **B10-03, A18-02 and B13-03** and a good NPHI – RHOB crossover in the wells **A12-03, A18-02, B13-03 and B13-04.**

In the wells B17-05, B17-06, F01-01 and F02-06 there is no evidence of gas accumulation is this seismic stratigraphic unit; it is present in shallower depths for which is no longer possible to observe any indicator of hydrocarbons.

The seal of this possible gas-bearing layers belong to the seismic stratigraphic unit s13. In the majority of the wells there is an abrupt change in the Gamma Ray values between the top of s12 (around 67 API) and the base of s13 (90 API).

As Gamma ray is a measurement of the natural radioactivity of the formation and hence normally reflects the clay content of the formation; it can be an indication of change in the granulometry in the units and therefore a change in the energy of deposition. Also the lithological description in the mudlogs show a change from siltstone – sandstone to claystones.

3.1.2. Seismic stratigraphic unit s11

There was found NPHI – RHOB cross-over evidence in the base and middle of the unit in the wells **A12-03, A18-02, B13-03 and B13-04** and DHIs in the wells **A12-03, A18-02, B10-03, B13-03 and B17-05**.

One difference with respect to the previous seismic stratigraphic unit (s12) is the fact that the possible seals belong to the same unit. Although the change in the gamma ray values between the possible gas-bearing layer and the seals are not that evident such as in the previous one, there is still possible to identify the different lithologies.

3.1.3. Seismic stratigraphic units s10 and s8

As is possible to see in There was found a very NPHI-RHOB in the wells A12-03 and A18-02.

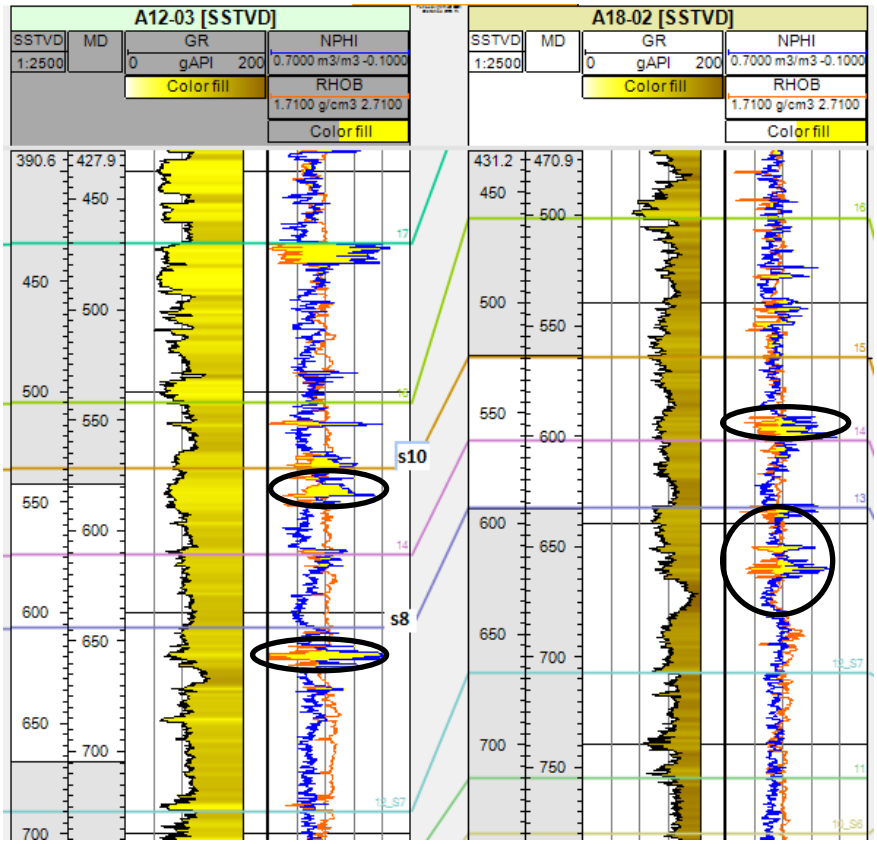

Figure 3-1. NPHI – RHOB cross-over of wells A12-03 and A18-02

There were also found DHI's and gas peaks in the well B10-03. The seals of the possible gas accumulations in s10 are located in the same seismic stratigraphic units, while the ones of s8 are located in the unit above (s9).

3.1.4. Seismic stratigraphic units s5 and s6

s5: Although there was not possible to find a good cross-over in none of the wells there were found DHI's in almost all the wells: **A15-04, B10-03, B13-03, B13-04, F01-01 and F02-06**

s6: as in the previous sequence there was not found any clear NPHI-RHOB cross-over in any of the wells; but there were found very good gas peaks and DHI's in the wells **A15-04, B10-03, B13-03, B13-04, B17-05 and B17-06.**

One characteristic that is important to mention is that the DHI's found in s6 in the well B17-06 is associated with a fault and is located in the shallower part of the unit with depth range oscillates around 500 to 950m.

In the seals of the possible gas-bearing accumulations were found very high Gamma Ray values (150 API) particularly in the well A15-04. Is important to mention that there is also an evident change between the Gamma Ray values of the seal and the reservoir which indicates a change in lithology and therefore in the energy of deposition.

3.2. Clay fraction, Effective stress and Porosity

3.2.1. Shepard's diagram

Traditionally, in geology the sediments are divided into four size fractions that include gravel, sand, silt, and clay, and are based on ratios of the various proportions of the fractions. Definitions of the fractions have long been standardized to the grade scale described by Wentworth in which gravel-sized particles have a nominal diameter of 2 mm; sand-sized particles have nominal diameters from <2 mm to >62.5 µm; silt-sized particles have nominal diameters from <62.5 µm to >4 µm; and clay is < 4 µm.

From the grain-size distribution of each samples, using the **clay as particles < 8 µm** taken from the laser diffraction analysis, was built the Shepard's ternary diagram to describe the approximate relationship between the size fractions:

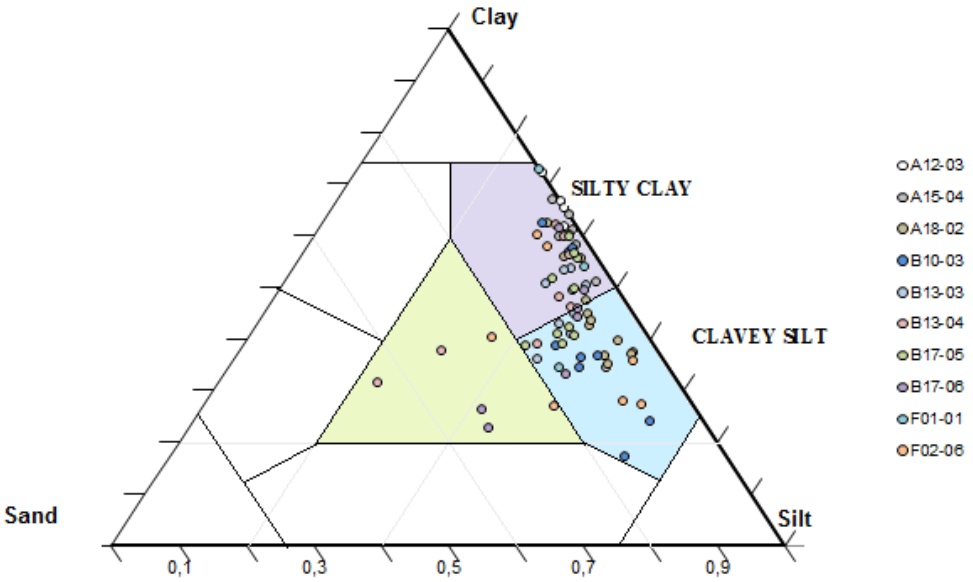

Figure 3-2. Ternary diagram (Shepard, 1954) showing the grain-size distribution for samples from the wells A12-03, A15-04, A18-02, B10-03, B13-03, B13-04, B17-05, B17-06, F01-01 and F02-06.

In the Figure 3-2 is possible to observe that the majority of the layers according to their size fractions relationships can be classify as **Silty clay** and **Clavey silt** with few points in **Clay-silt-sand .**

The sediments distribution in the Figure 3-2 show that the mudstone layer are poorly sorted; any of the layers sampled can be classified with just one type of sediment because although the clay content is the predominant in the layers, the silt particles also have an important influence.

The standard deviation parameter obtained by the grain-size analysis also gives an indication of the sorting in the sampled layers; from that analysis was obtain that from the 77 samples 52% are poorly sorted and the other 48% very poorly sorted.

This characteristic is normally attributed to the maturity and depositional environment of the sediments. Sediment Maturity refers to the length of time that the sediment has been in the sedimentary cycle. A poor sorted sediment can be also classified as immature sediment which means that has been short time in the sedimentary circle.

There is possible to attribute the sorting and maturity to specific depositional environments, being one of them de Glacial environment.

From literature as is possible to see in Figure 3-3 the majority of the age of the sampled layers corresponds to the Gelasian (early Pleistocene). There were defined five paleoenvironments in the area of study: Open marine temperate, transitional, restricted marine, shallow marine artic and fluvial, deltaic to paralic. (Wong, De Lugt, Kuhlmann, & Overeem, 2007)

The Neogene is a period of rapid filling and consequently shallowing in the North Sea Basin. In the Middle Miocene a delta system started to evolve from the east; progradation of the delta resulted in several major sequences within the Upper Cenozoic section in the North Sea Basin. One major sequence boundary is the Mid – Miocene Unconformity which is a transgressional surface that is characterized by sediment starvation during the late Middle Miocene; this sequence represents also the lower boundary of the study area.

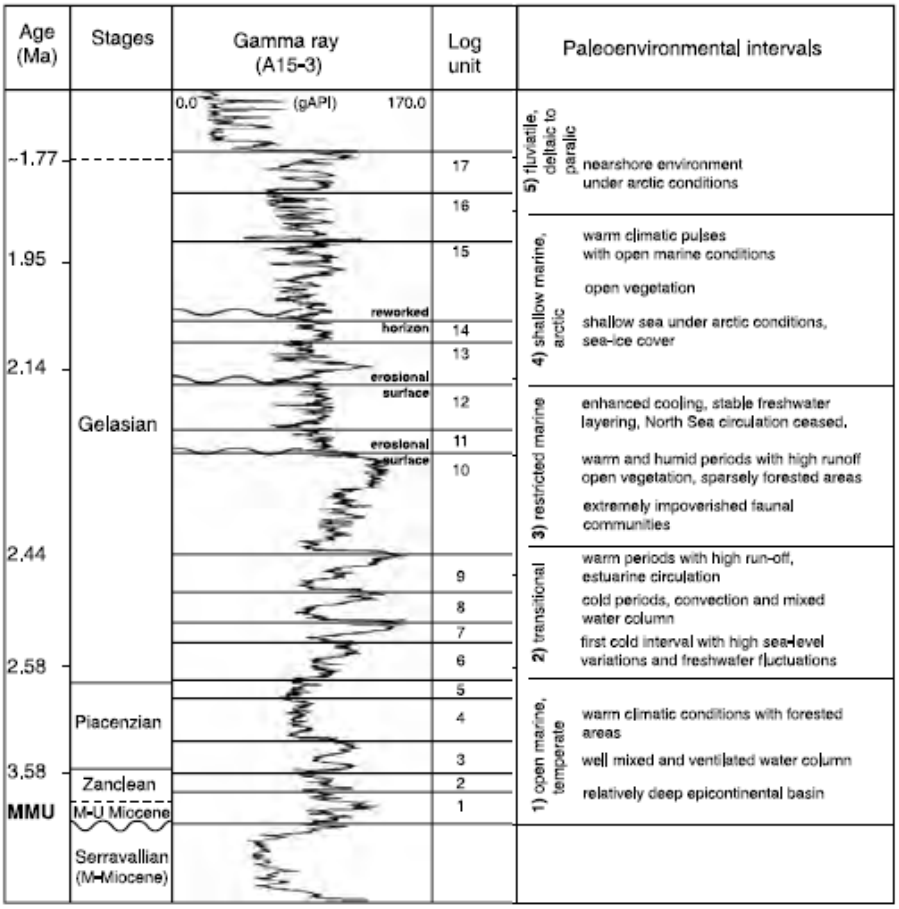

Figure 3-3. Paleoenvironmental interpretation compared with gamma Ray response of late Cenozoic interval of well A15-03 in the northern offshore (Wong, De Lugt, Kuhlmann, & Overeem, 2007)

The majority of the possible gas-bearing layers were found in the log units **17, 16, 15, 13, 10 and 9,** which corresponds to shallow marine to deltaic and form transitional to restricted marine respectively.

As a seismic stratigraphic unit is a record of cronostratigraphic, depositional and structural patterns and not a record of the time-transgressive lithostratigraphy, is only possible to associate the gas accumulation to specific genetically related strata.

3.2.2. Clay fraction vs seismic stratigraphic units location

There were plotted the clay fraction over the depths of each seismic stratigraphic sequence defined. This was made with the purpose of identified some relation between deposition and clay content of the layers.

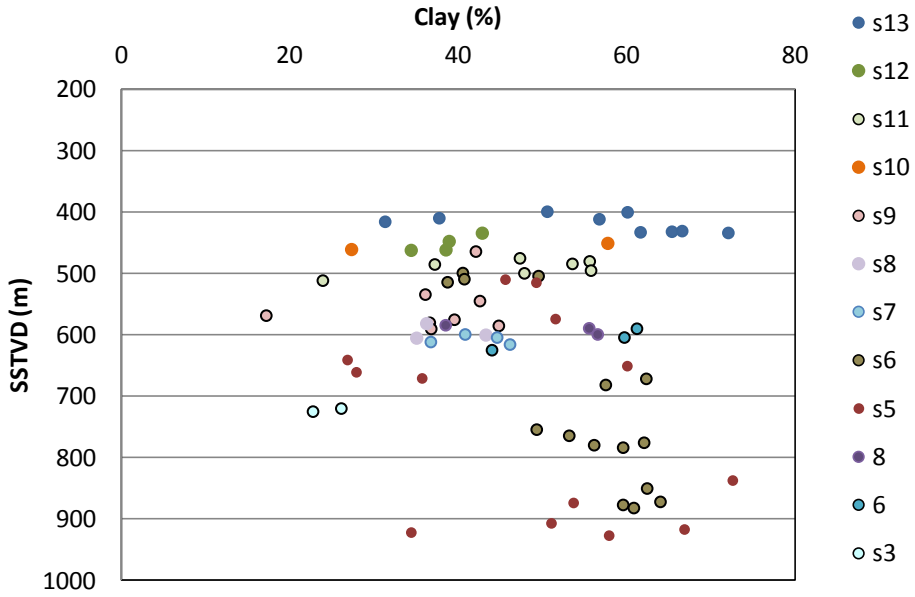

Figure 3-4. Clay content measured from grain size analysis by laser diffraction

In general, as is possible to observe in the figure above, even there are seismic stratigraphic sequences with high clay percentage reaching values higher than 70 %, are found 2 principal tendencies in the clay percentage among the seismic stratigraphic units: around 40 and 60 %.

There is a high amount of data points which values oscillates around 40% of clay principally in the units s12, s9, s8 and s7; what is also notorious is that there are located just between 400 and 600m SSTVD.

For the contrary the data points with the second mayor tendency of clay content (60%) are covering all the depth range of the study; from 400 from almost 950m SSTVD. The seismic stratigraphic units with this clay percentages are s13, s11, s5 and s6.

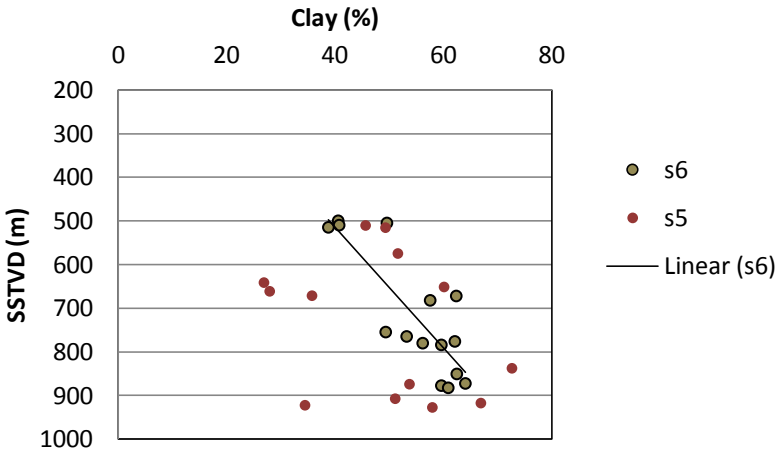

Figure 3-5. Clay content calculated of s5 and s6.

Is also possible to observe that in some units the clay content increase with depths, such as s5 and s6 previously mentioned. Its variation goes from 40 to 64% in the case of s6 and from 27 to 73% in the case of s5.

3.2.3. Porosity

According to the clay definition used in soil mechanics by Skempton (1970), Burland (1990) and Yang and Aplin (2004) in which clay are particles with a diameter less than 2µm were obtained the following results:

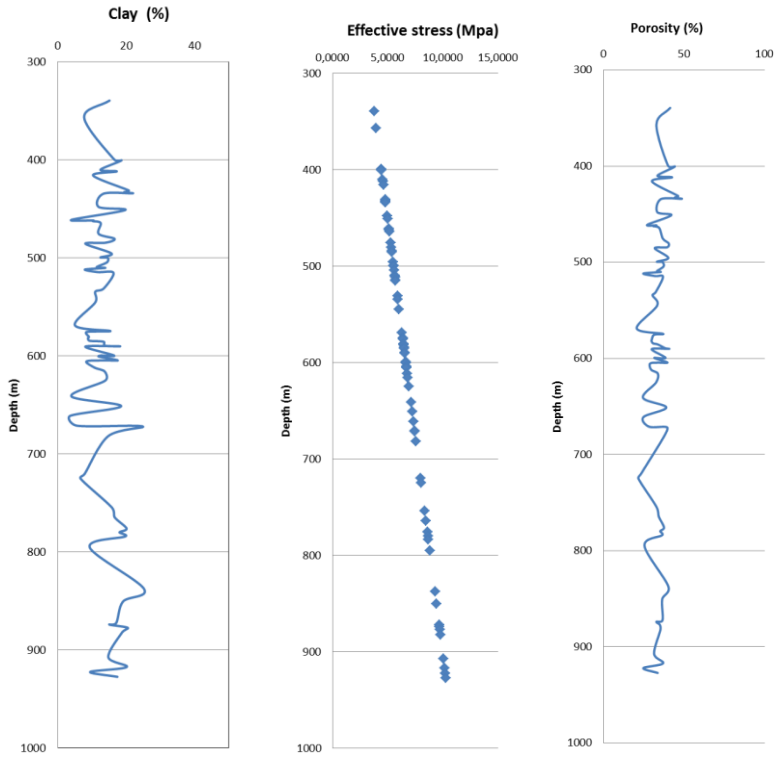

Figure 3-6. Clay content, effective stress and porosity of the mudstones layers

This previous graph is a compilation of all the samples covering the location of 10 wells at shallow depths between 300 and 1000m SSTVD. Is possible to observe that both the effective stress and the clay content have an influence in the porosity variation.

An increment of clay content at very shallow depths increase the porosity while an increment of the effective stress decrease it. For this reason is possible to observe in the Figure 3-6 that the general tendency of the porosity behaviour follows the opposite trend of the effective stress, being the specific variations product of the clay content.

Finer the material, the higher is its initial porosity but also the greater is the compaction rate. Therefore, finer-grained mudstones, thus, lose porosity faster with increasing effective stress than do coarser-grained mudstones. As a result, the porosities of sediments with different clay contents converge at high levels of effective stress. (Aplin & Yang, 2004)

For the porosity calculation were used the approach of Yang and Aplin (2004) and Burland (1990), obtaining the compression coefficients by different formulations.

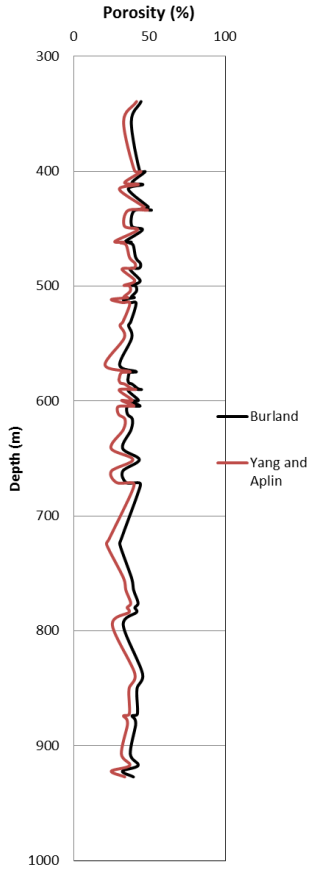

Figure 3-7. Yang and Aplin (2004) vs Burland(1990) porosity

The black line in the figure represents the porosity calculated by the Burland (1990) approach and the red line, the porosity calculated by the Yang and Aplin approach (2004).

The values obtained by the Burland datasets show less change and higher porosity for the same clay content. Both values have high porosities with respect to the literature found, especially in the shallow layers.

Porosity from literature

The samples were taken for depths between 300 to 1000m SSTVD in the Dutch northern offshore. According to the literature, the deposition of this sediments occurred after the **Mid Miocene Unconformity** belonging to the Upper North Sea Group.

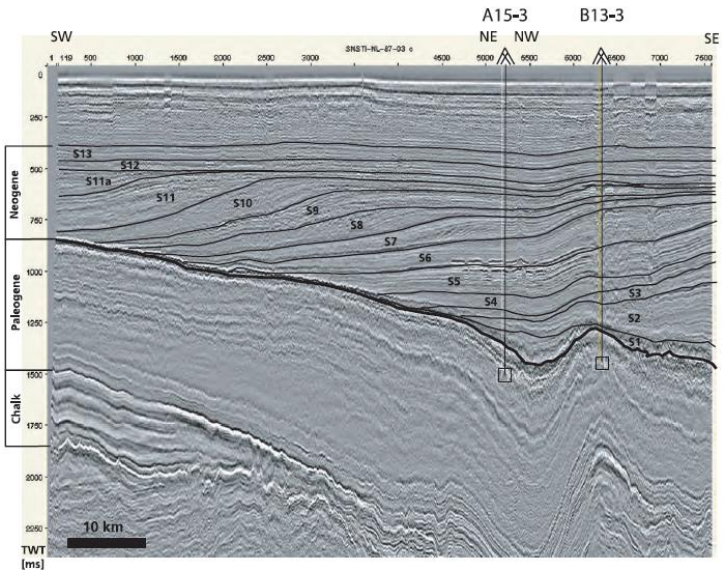

Figure 3-8. Seismic section in northern offshore blocks A, B and E showing prograding character of Upper Cenozoic deposits. Thirteen seismic units (S1 to S13) are indicated; the lower boundary is the Mid Miocene Unconformity (MMU)(Wong, De Lugt, Kuhlmann, & Overeem, 2007)

Agreeing to the Figure 3-8 the age of deposition of the study area corresponds to the **Neogene** and **Quaternary** which could correspond to the ***Breda formation*** (Miocene, locally Pleistocene), ***Oosterhout / Maassluis Formation*** (Pliocene – Pleistocene) and other various ***Quaternary formations.***

The Oosterhout formation can be defined as a **Succession of sands, sandy clays, and grey and greenish clays**. The upper boundary of the Oosterhout Formation is, in most places, taken at **the top of a series of clay beds, which are overlain by shelly, fine-grained to coarse-grained sand with sparse clay intercalations** and form part of the Early Pleistocene Maassluis Formation.

The formation is present in the central and western Netherlands (with the exception of the extreme southwest), and the **entire offshore area.** It was deposited in a shallow-marine environment, partly in a delta-front setting and partly in an inner-neritic setting.

Source	***Depth (m)***	***Formation***	***Porosity (%)***	***Clay content(%)***	***Others***
	470,1	-	33,2	-	
1*	471	-	32,5	-	
		Various			
	-	**Quaternary**	**35 - 40**	-	
	-	Oosterhout	35	-	
2*	-	Breda	27 - 30	-	
	162 - 252	Oosterhout	33,7 - 37,2	0,6 - 15,5	
	255		29,8	18,4	
	258	Breda	27,3	13,7	Onshore
3*	426 - 478		-	10,2 - 18,7	
	-	Oosterhout	35	0 - 10	
4*	-	Breda	27,2	10,1 - 19	

Table 3-1. Porosity and clay content values in the study area taken from literature.

*Where 1*is NL Oil and gas portal, 2* is the Rijks Geologische Dienst (1996), Nederlands Instituut voor Toegepaste Geowetenschappen TNO (1998) and the Rijks Geologische Dienst en TNO (1983, 1984); 3*TNO-rapport Geomechanische, geochemische en geohydrologische eigenschappen van Tertiaire kleipakketten – CAR Fase II, Bijlage Q and 4*is the TNO-rapport Geomechanische, geochemische en geohydrologische eigenschappen van Tertiaire kleipakketten – CAR Fase II, tabel 7.*

As the results from both methods are very similar, was chosen the one proposed by (Aplin & Yang, 2004) because the porosities are quite lower and the equations are derived from a relatively high number of data points covering the full range of clay content and a much larger range of effective stress.

The shallower layers have high porosities (around 45 %); this can be explain due to the fact that are very shallow unconsolidated sediments with high clay content. Although the clay particles have a high compaction rate than the other types of sediments it initial deposition occurs with a high porosity, sometimes reaching values of 60%. As increase the depths, the porosity is decreasing because the raise in the effective stress make the clay to compact.

3.3. Permeability and pore-throat size

In order to calculate the mudstones permeability's were used the values of clay fraction and void ratio (porosity). The permeability values obtained are very low oscillating between 0.000064 and 0.006463 mD (6.36 E-20 – 6.37 E-18 m^2).

There were obtain three different pore radius for each layer: the values calculated by the equivalent grain size method using the median grain size are from 0.43 to 1.43 µm; except for one data point which value is too high compare with the rest (2.37µm). As is possible to observe in Figure 3-9 was built a relationship between the pore throat size calculated by the equivalent grain size method and permeability. The majority of the permeability values are between 0.000064 and 0,0004 mD which follow a very clear trend.

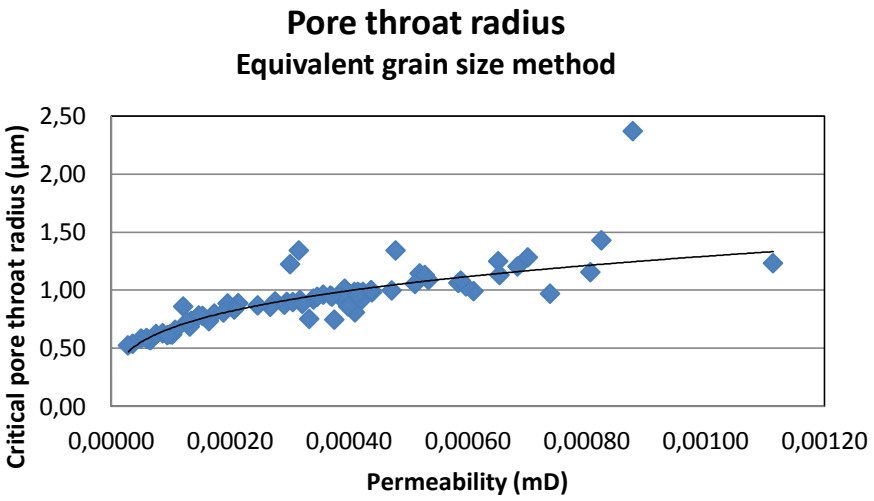

Figure 3-9. Permeability- Pore Throat radius relationship from the equivalent grain size method

Plotting the same previous data in with a log scale is possible to see an exponential trend between the values, obtaining the following equation with a R^2 of 0.7753:

$$r = 9.1904 * k^{0.2841} \qquad \textbf{(33)}$$

In which ***r*** *is the pore throat radius in µm and* ***k*** *is vertical absolute permeability in mD.*

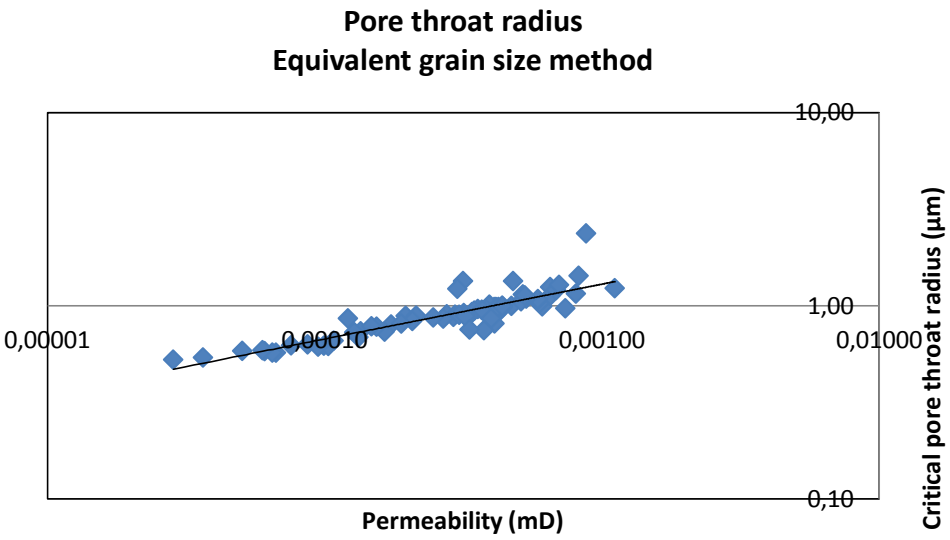

Figure 3-10. Permeability- Pore Throat size relationship from the equivalent grain size method (log-log scale)

$$log(r) = 0.2841 * log(k) + 0.9933 \qquad \textbf{(34)}$$

*In which **r** is the pore throat radius in µm and **k** is vertical absolute permeability in mD.*

What is possible to observe in the figures above is that almost all the data points are following a very good trend; except for 5 data points showed in red. Relating the former points with the lithological characterization was found that that that samples are the only ones classified as **sand-clay-silt** in the Shepard diagram showed in figure 34 (contain at least 20% sand) from 77 samples taken.

As the calculation of the permeability was made from as empirical equation for mudstones, the permeability values for the 5 data pointes previously mentioned is not very reliable.

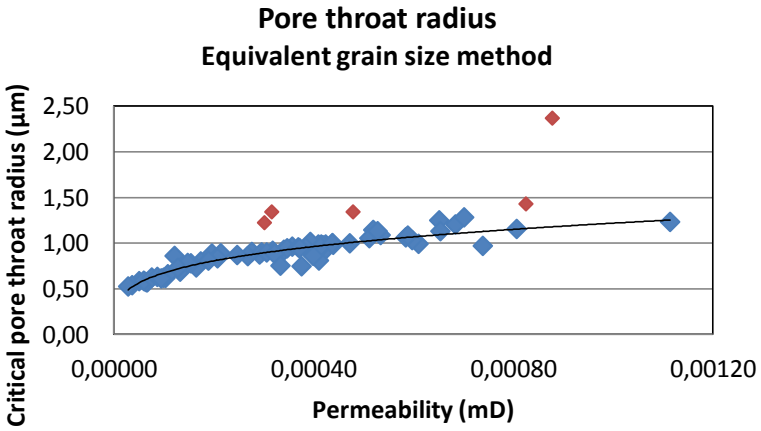

Figure 3-11. Permeability – Pore Throat relationship with a lithological constraint

Adding the constraint to the samples of sand content < **20%** was found the following relation with a $R^2 = 0.8948$:

$$log(r) = 0.8593 + 0.2579 * log\,(k) \qquad \textbf{(35)}$$

The second values of pore throat size were calculated using the mean grain size of the grain-size distributions. The values obtained oscillate between 0,48 and 1,17µm, except for two data points which values are too high compared with the rest (2 and 2,53µm).

There were also built a relation between this pore throat values and the permeability, as is possible to observe in the Figure 3-12

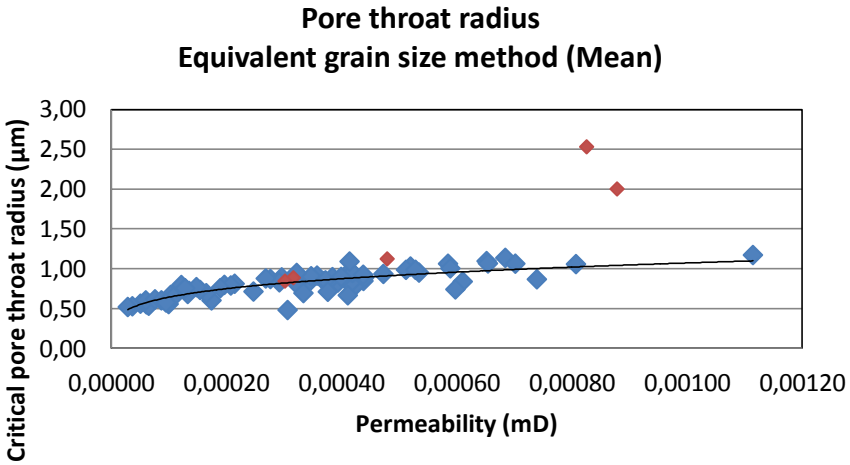

Figure 3-12. Permeability – Pore Throat relationship Mean

Adding also the constraint to the samples with sand content < **20%** was obtain the following relation with a R^2= 0.7097

$$\log(r) = 0.6983 + 0.2226 * \log(k) \qquad \textit{(36)}$$

The third values of pore throat size were obtained for comparison from the permeability values using Equation 0. From this relationship were obtain lower values of pore throat radius which are between 0.10 to 1.39 µm as is possible to see in Figure 3-13

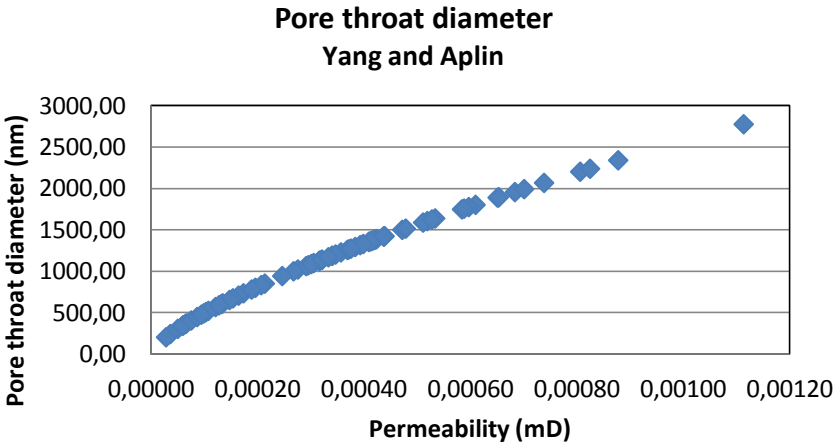

Figure 3-13 . Permeability- Pore Throat size relationship

Even the pore throat radius calculated by the previous equation are lower, there are still in the same order of magnitude. This is a good indicator that the values obtain by the grain-size method are quite reliable.

Although permeability doesn't have a direct influence in the seal capacity estimation, it is useful for modeling rates through seals and for predict fluid pressure.

From the petroleum exploration point of view, fluid flow through mudstones critically manifest itself as the leakage of hydrocarbon through cap rocks or as vertical migration to stratiphically higher prospects.(Aplin & Larter, 2005).

In some models (Ingram, Urai, & Naylor, 1997), the top seal dynamics is performed using the simply Darcy flow equation:

$$Q = \frac{\Delta P}{\mu}\frac{kA}{\Delta l} \qquad (37)$$

In which Q is the flow rate, ΔP is the buoyancy pressure (MPa), A is the leak window area (m^2), μ is the viscosity of the fluid and Δl is the seal thickness (m).

Observing the previous equation is possible to notice that lower the permeability, lower is going to be the leakage of the seal. There also possible to mention than the thick of the seal, like the permeability, doesn't have influence in the sealing capacity; but appears in the calculation of the leakage out of the seal.

It has been demonstrated by (Ingram, Urai, & Naylor, 1997) that capillary entry pressures are not the only control on max column height in top seals when there is a leakage scenario

In our case the permeability values are fairly low (10^{-20}- 10-^{18}), which is very good to control the seal leakage. There is a good possibility that due to the low permeability, once capillary seal has been reached the flux into the traps will be always greater than the flux out of trap. The accumulating column of hydrocarbons will therefore always have a buoyancy force greater than the capillary entry pressure, which renders the capillary seal ineffective. The result is that leakage is controlled by the permeability of the seal rock alone.

3.3.1. Pore throat radius and seismic stratigraphic units

It was plotted the pore throat radius over depths for each seismic stratigraphic unit present in the study area.

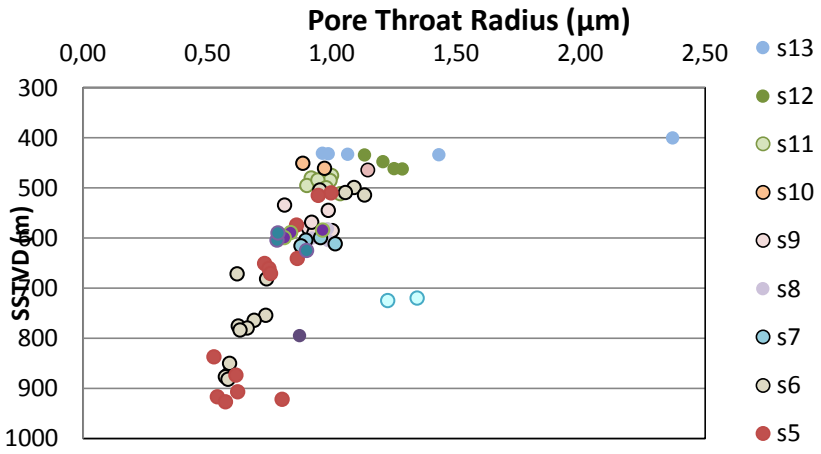

Figure 3-14. Pore throat radius over depth with the seismic stratigraphic units

What is possible to observe in the figure above is that as expected, the pore throat radius are following a very clear trend over the depth; as the depths increase the size of the pore throat decrease.

This trend can be explained due to the fact that the pore throat radius were calculated with the equivalent grain size method in which porosity is an essential parameter in its calculation.

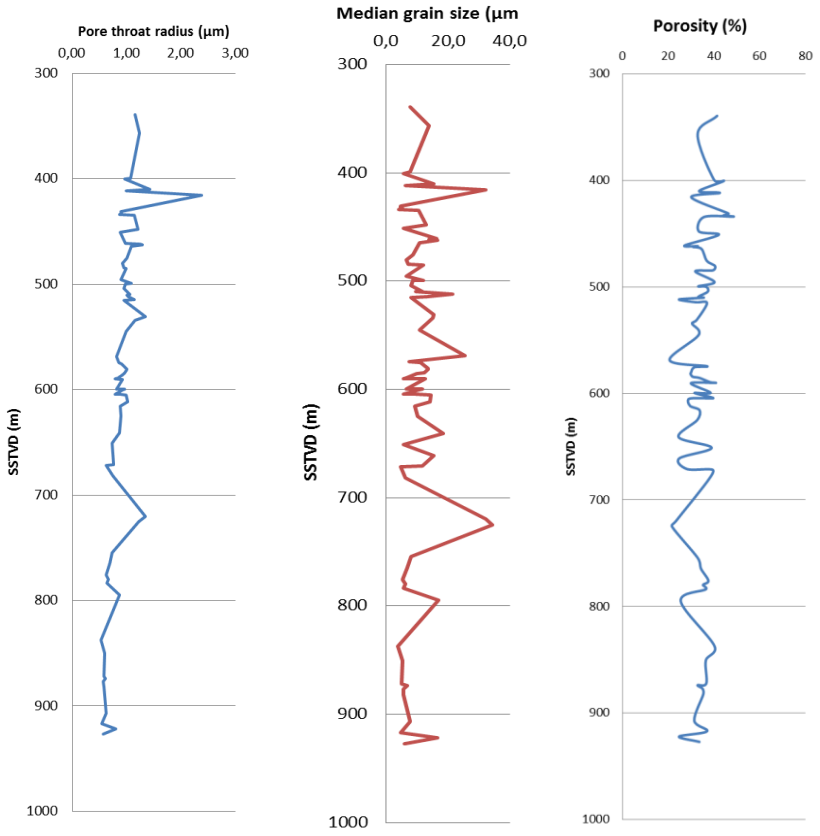

Figure 3-15. Comparison between pore throat radius, median grain size and porosity

From the Figure 3-15 is possible to observe that the pore throat radius is following a very similar trend over depth with respect to the Median grain size and a opposite trend with respect to porosity.

Although for the calculation of porosity it was not used the median grain size, it is strictly related with the clay content. If the clay content is higher the median grain size will be lower because it represents the particle size in which half of the population is finer than. For this reason is possible to observe that the three trends have very similar characteristics.

3.4. Threshold Capillary Entry Pressure

The threshold capillary entry pressures of the mudstones layers were calculated for the mudstones layers sampled. The values oscillates between 0.06 MPa (8 psi) and 0.24 MPa (35 psi).

From the Capillary retention- facies ranking of the Pe in Hg/air system is possible to compare the values calculated and therefore the type of rock that should be present in our area of the study according to the scheme in Figure 3-16

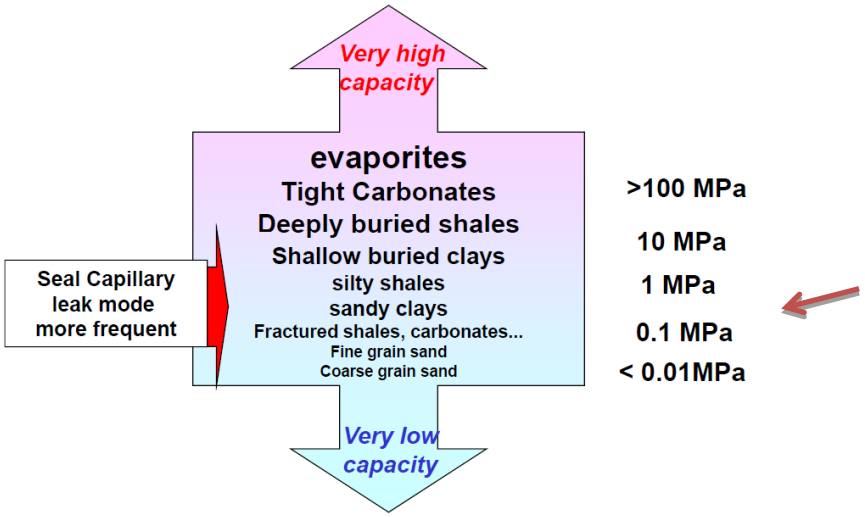

Figure 3-16. Capillary retention facies ranking

According to the scheme above, the lithology of the samples should correspond to sandy – silty clays. Making reference to the Figure 3-2. Ternary diagram (Shepard, 1954) showing the grain-size distribution for samples from the wells A12-03, A15-04, A18-02, B10-03, B13-03, B13-04, B17-05, B17-06, F01-01 and F02-06., the majority of the samples were characterize as Silty clay and clavey silt, for which there is a good agreement between the lithology and the leak mode expected and the one related with the calculated capillary entry pressure.

As the permeability and the capillary entry pressure of mudstones at a given porosity are strongly influenced by lithology or grain-size distribution is also possible to establish a relation between them.

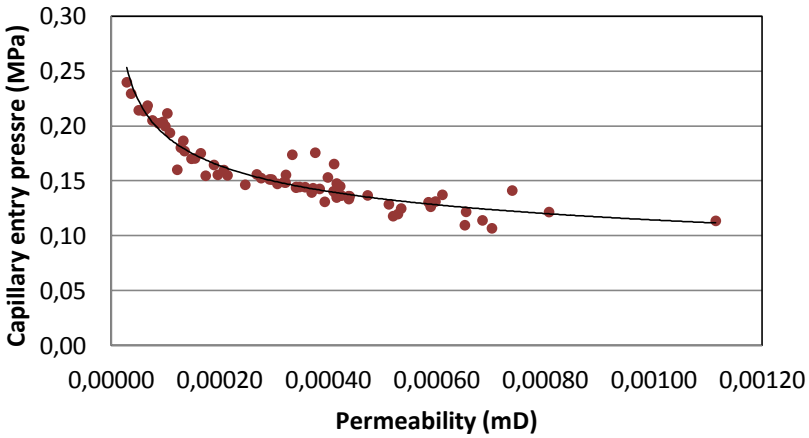

Figure 3-17. Relation between Pce and permeability

There was built a relation between the calculated capillary entry pressure and the permeability, taking out the data points with sand content > 20% taking in consideration the lithological constraint exposed in the subchapter Permeability and pore-throat size.

$$\log(Pce) = -0.224 * \log(k) - 1.6126 \qquad \textbf{(38)}$$

In which Pce is the entry capillary pressure in mD and k is the instrinsic absolute permeability of the medium

As expected was found a good regression coefficient of R^2 = 0.8862 because both parameters are strongly related to the diameter of the connected pore throats.

3.5. Sealing Capacity

3.5.1. Sealing Capacity vs SSTVD

From a compilation of all the well data was built the following graph:

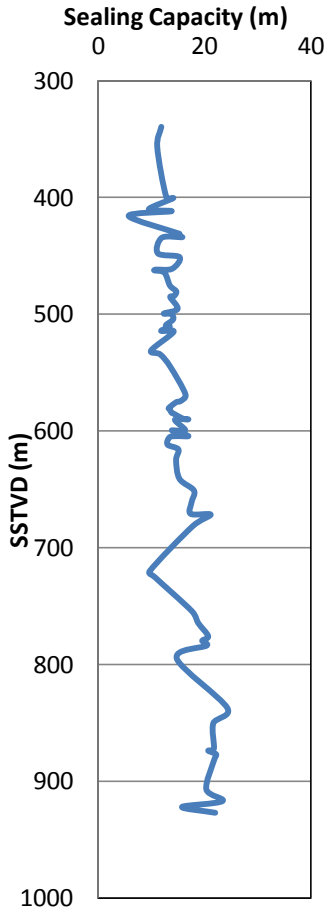

Figure 3-18. Calculated sealing capacity over depth

As is possible to observe in Figure 3-18, there is a general increasing trend of the seal capacity over the depth. The higher values of the seal capacity are found in the deeper part of the study area among 800 to 950m SSTVD . The general tendency of increasing seal capacity with the increse in depths can be explain because of the decrease of porosity and interfacial tension over depths; being both of them importants factor in the calculation of the sealing capacity.

The porosity, used to calculate the pore throat radius, as is possible to see in the Clay fraction, Effective stress and Porosity subchapter, decrease with the increase of the vertical efective stress which is linery related with the depth

As the porosity is an important factor in the calculation of the sealing capacity, it follows a similar tren over depths in the sense that a decrease in porosity causes an increase in seal capacity, what is show in

Figure ***3-19.***

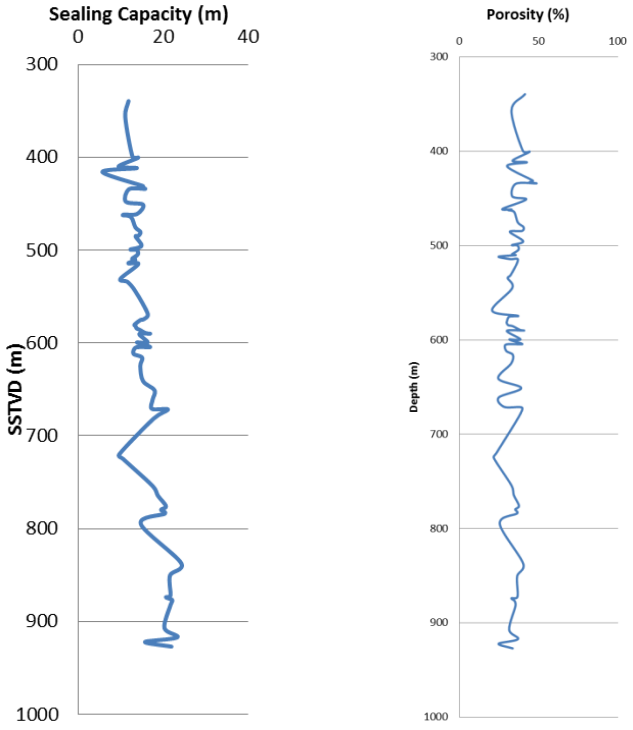

Figure 3-19. Comparison between sealing capacity and porosity trends.

There is also possible to observe in Figure 3-18 that there are some specific depths in which the seal capcity seams to decrease with respect to the average values; this can be notice around 400, 700 and 800m. The higher concentration of data points can be seen around 500 and 600m in which the seal capacity is following the general trend.

The previous variations can be explained due to the presence of other factors that influence the calculation of the maximun hydrocarbon column that the seal can retain such as the mean grain size of the mudstones layers and the clay content.

3.5.2. Sealing Capacity vs seismic stratigraphic units

In order to find the possible relation between the sediments deposition and the sealing capacity was plot the sealing capacity over the different seismic stratigraphic units defined in the logs.

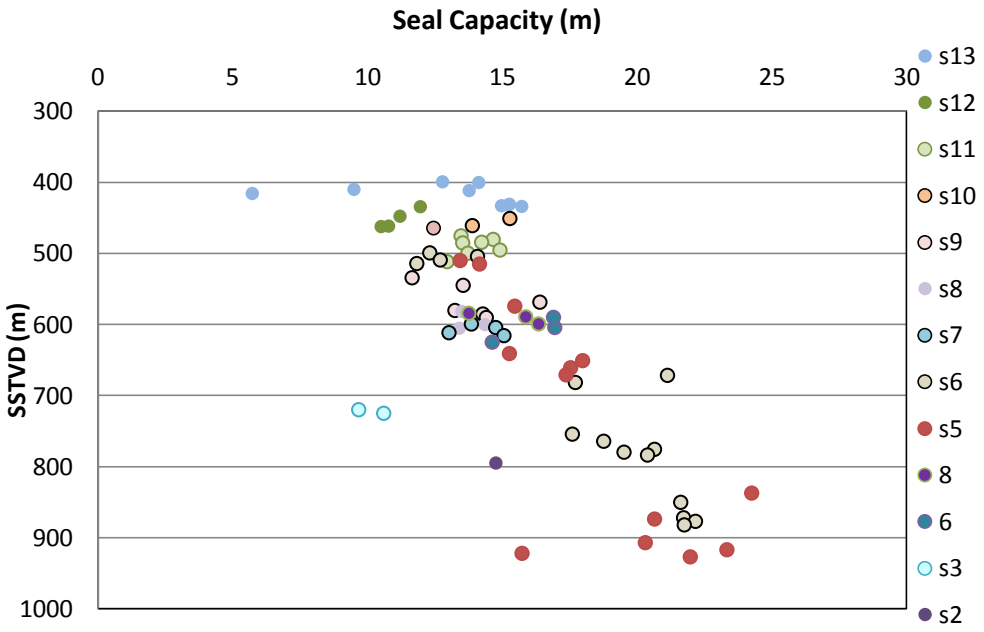

Figure 3-20. Calculated Sealing Capacity over SSTVD showing the seismic stratigraphic units

As was expected, it was found an opposite trend with respect to the pore throat over SSTVD (Figure 3-14). Higher the pore throat radius, lower is the sealing capacity of a formation because less pressure is going to be needed for the flow to pass throw the pores.

Is also possible to see in the Figure 3-20 there is some relation between the Seal Capacity and the seismic stratigraphic units. Also there are some units such as s7

and s3 with less data available which means that there was a poor indication of gas accumulation in the layers below.

The principal seismic stratigraphic sequences that can be mention are:

- **s13**

The sealing capacity varies from a few to 16 meters. Although this seismic stratigraphic unit is found at very shallows depths its sealing capacity is still good compare with the rest.

The lower values can be explain due that as is possible to see in Figure 3-21, the layer is very thin (around 6 meters) and the samples were taken just in the top and bottom border of the layer.

These two data points present a high percentage of sand (> 20%) which may explain it low seal capacity.

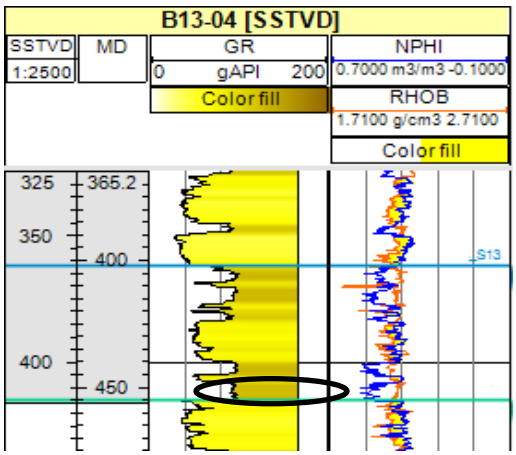

Figure 3-21. Layer sampled of the seismic stratigraphic unit s13 in the well B13-04.

- **s12, s11, s10, s9 and s8**

The sealing capacity of this sequences follows the increasing general trend with depths.

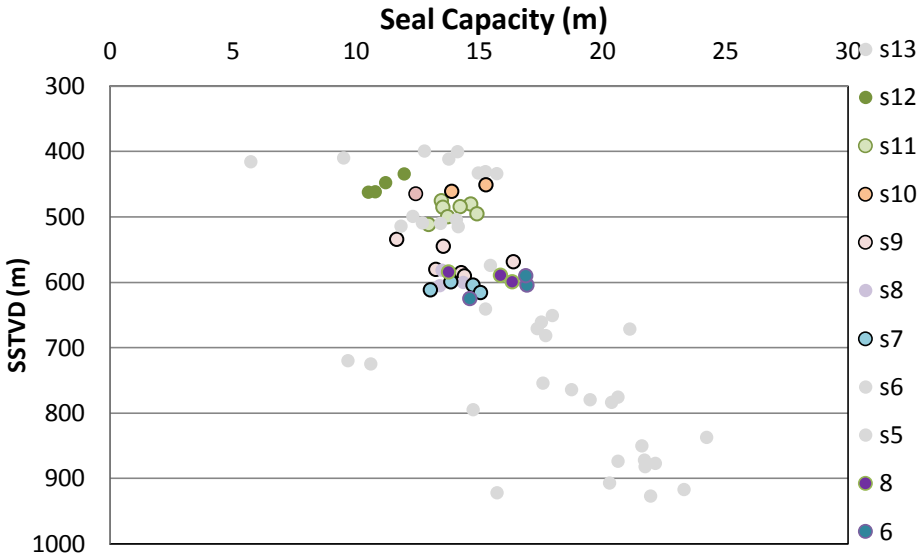

Figure 3-22. calculated seal capacity of s12, s11, s10, s9 and s8

Even if in some seismic stratigraphic units were taken just a few samples, is possible to observe in the figure above that they are following the same trend that the others. It sealing capacity range is around 8m, varying from 11 to almost 18 m of sealing capacity.

- **s5 and s6**

The best characteristic of these seismic stratigraphic sequences is the fact that covers a wide depth range between 500 to 930 approximately. The sealing capacity of both at the deeper layers is very good oscillating around 35m and even reaching more than 40m in some cases (s5)

There is also found a good relation between the depths and the sealing capacity especially in s6; the deeper are the layers, higher is the amount of gas that they can retain.

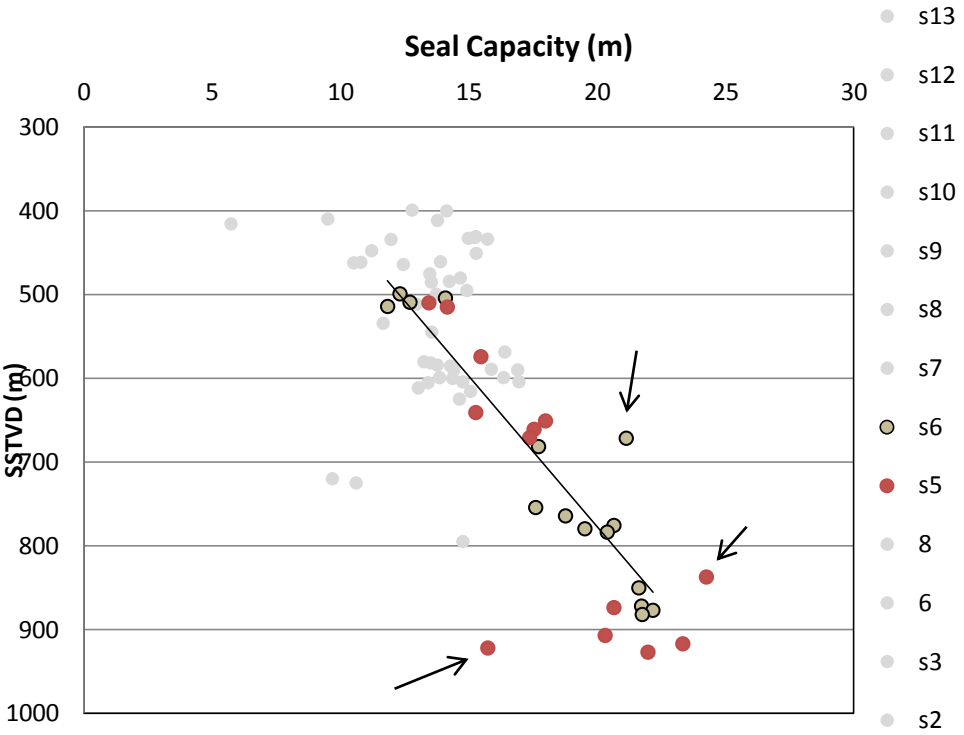

Figure 3-23. Calculated seal capacity of s5 and s6

The figure above shows the relation between the sealing capacity and the depths of the seismic stratigraphic sequences s5 and s6. The s6 presents a more clear linear tendency in all the data points.

Although s5 also present a linear trend in the seal capacity with respect to the SSTVD, the data pointes are less align specially in the deeper part of the study area.

In s5 there is possible to point out 2 data points which deviate the linear tendency with depth of this seismic stratigraphic unit. The first is a data point which seal capacity is lower to respect to the tendency (922m depth); this measurement was taken from the same layer and well (A15-04) that the other points at similar depths (907, 717 and 927m) which have a higher seal capacity.

Being the clay measurements obtain from this samples considerable lower that the others samples taken in the same layers and that the log data doesn't show any possible change of lithology due to the presence of a leaky layer; is possible to infer that the sample could be contaminated and the measurement is not reflecting its real clay percentage.

The second data point has a higher seal capacity with respect to the rest measurements at the same depth (837 m); it can explain due that the sample was taken from a different well (F01-01) and its clay content is high with respect to the rest.

In the sequence s6 there is one measurement that is deviated from the linear tendency of depth with respect to seal capacity. This data point show a higher seal capacity because its median grain size is very low compared to the rest.

3.6. Sealing capacity by pressure data

There was obtained the sealing capacity by pressure data in 5 wells (A12-03, A18-02, B13-03, B13-04 and B17-06)

3.6.1. A12-03

SSTVD (m)	Hydrocarbon column (m)
433.27	9.47
530.27	20.54

Table 3-2. hydrocarbon column calculated by pressure data in the well A12-03

From the well A12-03 were obtained just two measurements of hydrocarbon columns corresponding to the area of study.

3.6.2. A18-02

SSTVD (m)	Hydrocarbon column (m)
503.12	7.7
556.62	14.14
592.22	4.05
611.12	13.5

Table 3-3. hydrocarbon column calculated by pressure data in the well A18-02

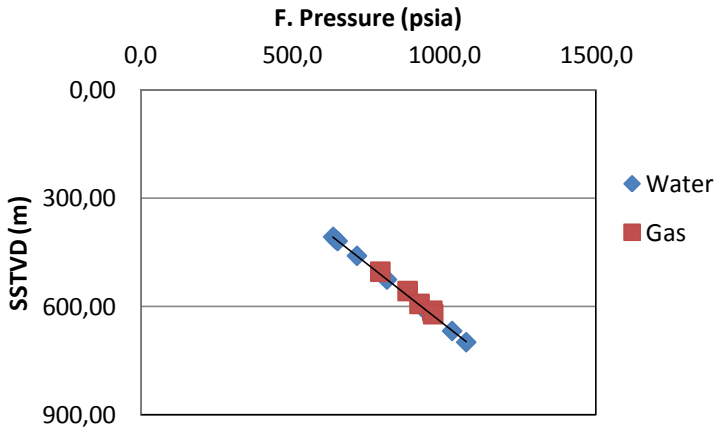

Figure 3-24. Water pressure gradient well A18-02

The availability and the quality of the pressure data in the previous well was very good, and was possible to find four pressure measurements.

In the Figure 3-24 is not very clear the difference between the water and gas measurements; this can be explain because the gas pressure (over – pressure) is not very high with respect to the water gradient. This is consequence of the height of the hydrocarbon columns which values shown in Table 3-3 are quite low.

3.6.3. B13-03

SSTVD (m)	Hydrocarbon column (m)
340.39	5.59
495.89	13.57
609.89	10.37

Table 3-4. hydrocarbon column calculated by pressure data in the well B13-03

3.6.4. B13-04

SSTVD (m)	Hydrocarbon column (m)
351.4	9.53
518.9	17.02

Table 3-5. hydrocarbon column calculated by pressure data in the well B13-04

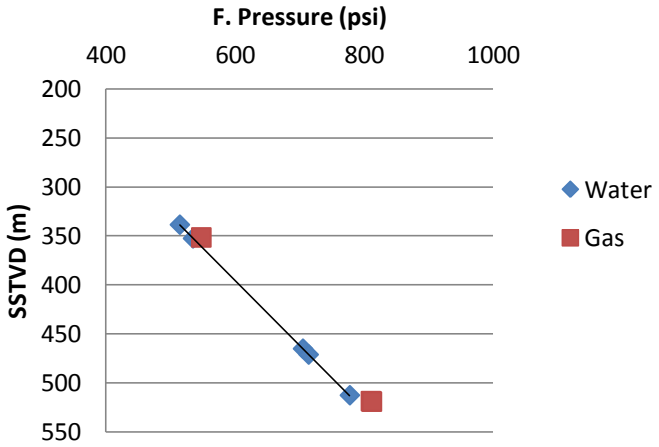

Figure 3-25.Water pressure gradient well B13-04

In the well B13-04 were found just gas pressure measurements in the area of study. As in the previous well the hydrocarbon columns calculated were not very high.

3.6.5. B17-06

SSTVD (m)	Hydrocarbon column (m)
631.25	9.33

Table 3-6. . hydrocarbon column calculated by pressure data in the well B17-06

The measurements in this well were very scarce so as a consequence was possible to obtain just one hydrocarbon column from pressure data.

3.7. Sealing capacity calculated by grain-size distribution vs hydrocarbon columns calculated by pressure data.

There were compared the results obtained by pressure data vs the ones obtain by grain-size distribution. In the following figures is shown the stratigraphic position of the layers sampled, and the cross-over between NPHI and RHOB as gas indicator.

Was also compared the height of the cross-over with the hydrocarbon columns calculated in order to see if there was any relation among them.

The tables blow shown the depths in which are located the seals, both MD and SSTVD and the values of hydrocarbon columns obtained by the different methods.

3.7.1. Well A12-03

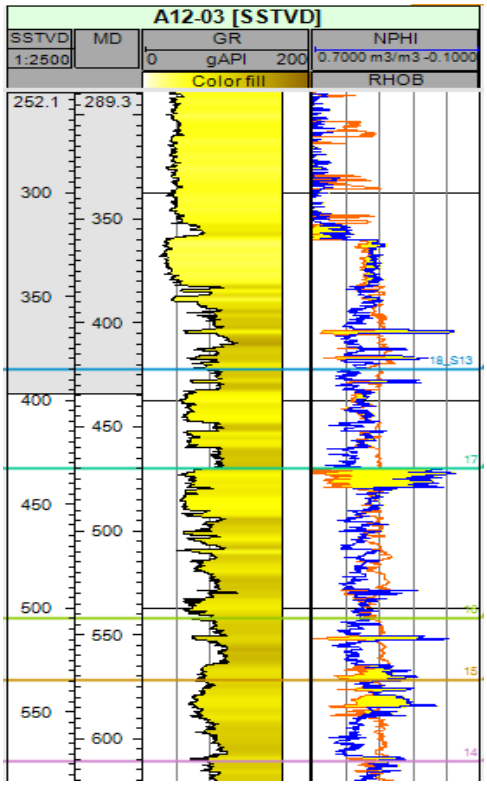

Figure 3-26. NPHI-RHOB well A12-03

MD (Seal)	**SSTVD (Seal)**	**Hydrocarbon column (m)** (Pressure data)	**Hydrocarbon column (m)** (Grain-size distribution)	**NPHI – RHOB Crossover (m)**
460 - 470	422.78 – 432.78	10	15	10 (+10)
543 – 550 553 - 564	505.75 – 512.75 515.75 – 526.75	21	-	22

Table 3-7. Comparison between hydrocarbon columns calculated by pressure data and by grin-size distribution of the well A12-03

As is possible to see in Table 3-7 there is good agreement between the hydrocarbon columns calculated by the different methods and the NPHI-RHOB found in the logs. The 10 (+10) in the first layers means that there is a very clear

cross-over in the first 10 m as is possible to see in the Figure 3-26 and in the second 10m there is still possible to observe a cross-over but less clear than before.

In the second layer (s12) there was not possible to calculate the sealing capacity from the grain-size distribution because the lack of cuttings or cores available. As is possible to see in the figure above there is also a correspondence between the pressure data and the cross-over in the logs. There is also important to mention that in the logs the cross-over is not totally continuous; although the total cross-over corresponds with the gas column measured by the pressure data, seems that there are thin sealing layers in the middle of the gas-bearing layer which was not perceived by the pressure data.

3.7.2. Well A18-02

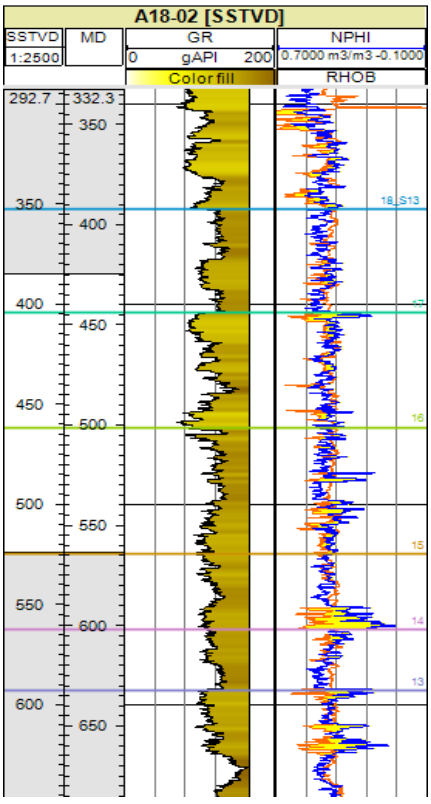

Figure 3-27. NPHI-RHOB well A18-02

MD (Seal)	**SSTVD (Seal)**	**Hydrocarbon column (m)** (Pressure data)	**Hydrocarbon column (m)** (Grain-size distribution)	**NPHI – RHOB Crossover (m)**
433 - 444	393.16 – 404.16	-	14	13
529 - 538	489.16 – 498.16	7	14	13 (+12)
580 - 591	540.16 – 555.16	14	15	16
620 - 631	580.16 – 591.16	4	14	6
643 - 649	603.16 – 609.16	13	14	15

Table 3-8. Comparison between hydrocarbon columns calculated by pressure data and by grin-size distribution of the well A18-02

As is possible to observe in the table above there is a very good match between the hydrocarbon columns calculated and the NPHI-RHOB cross-over. In the first layer (s13) there is no grain-size distribution data available but there is still a good agreement between the hydrocarbon column and the log data. In the second layer (s11) the cross-over seems bigger that the max. hydrocarbon column that the seal can hold; but there still an agreement between the most clear part of the cross-over and the values calculated.

What can also be seen form the crossover is that different from the well a12-03 is less clear, is appears like a possible intercalation between sealing a leaky layers. There is not a good accumulation in this interval.

In the third (s9) and last layer (s8), the agreement between the results is very good. Both calculations made with pressure data and grain-size distribution are matching perfectly between them and with the log data. The cross-over within this layers is also very good, showing a possible gas accumulation.

For the contrary in the sealing depth between 580 – 591m there is not a good agreement between all the values. The possible interpretation of the former results is that the sealing capacity of the rock is higher than the gas that is

accumulated; this means that could be a lateral migration instead of vertical or that the dynamic on the seal could reduce its seal capacity. Vassenden et al. (2003) used a laboratory experiment to study migration into a filling of a synthetic trap, followed by leakage of oil out of the same trap. The sequence of snapshots and plotted injection and production volumes documented that the trap started to leak as soon as the oil column exceeded the entry pressure of the cap rock. Thereafter, the oil column continued to increase in height but at a much lower rate. When the supply was stop the column started to shrink, until it stabilized at a column significantly below the column at which started to leak. (Sylta, 2005).

3.7.3. Well B13-03

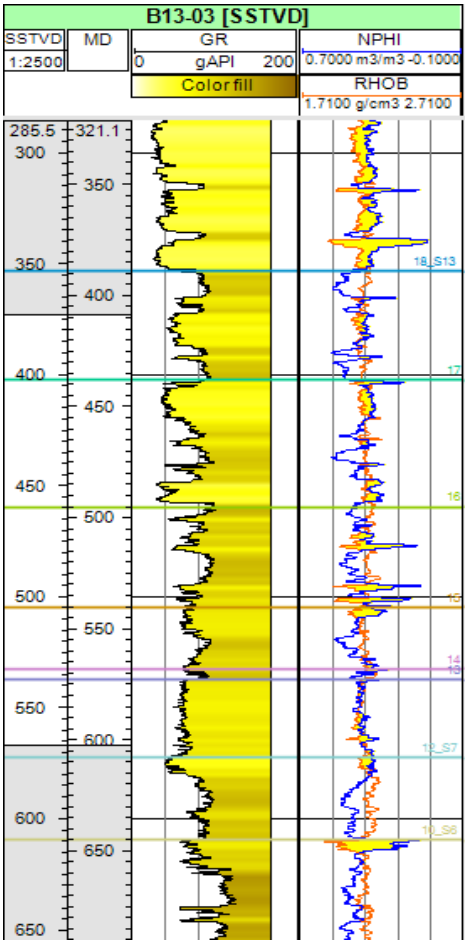

Figure 3-28. NPHI-RHOB well A18-02

MD (Seal)	**SSTVD (Seal)**	**Hydrocarbon column (m)** (Pressure data)	**Hydrocarbon column (m)** (Grain-size distribution)	**NPHI – RHOB Crossover (m)**
372 - 375.5	336.4 – 339.9	6	12	12
429 - 439	393.4 – 403.4	-	13	15
517 - 530	481.39 – 494.39	14	14	15 (+5)
554 - 573	518.4 – 537.4	-	12	14
636 - 645	600.4 – 609.4	10	15	7

Table 3-9.Comparison between hydrocarbon columns calculated by pressure data and by grin-size distribution of the well B13-03

In general there is a good agreement between the hydrocarbon columns calculated by pressure data and grain-size distributions and the NPHI – RHOB cross-over on the logs.

In the first, second and fourth layer (336 – 339m) and (393 – 403 m) respectively, the sealing capacity calculated from the grain size distribution has almost the same values than the cross-over in the logs.

The better match is found in the layer with depth is between 481 – 494m. Both the calculations made by pressure data and grain-size distributions agree with the log data.

Unfortunately the quantity of pressure data is this well is very poorly for which the calculated values are very scarce for make a good comparison.

As in the well B18-02 is found a sealing layer at 600 – 609 SSTVD in which the sealing capacity of the rock is higher than the gas accumulation shown by the logs and the pressure data. The possible explanation could be the lateral leakage or the dynamic of the seals previously mentioned.

3.7.4. Well B13-04

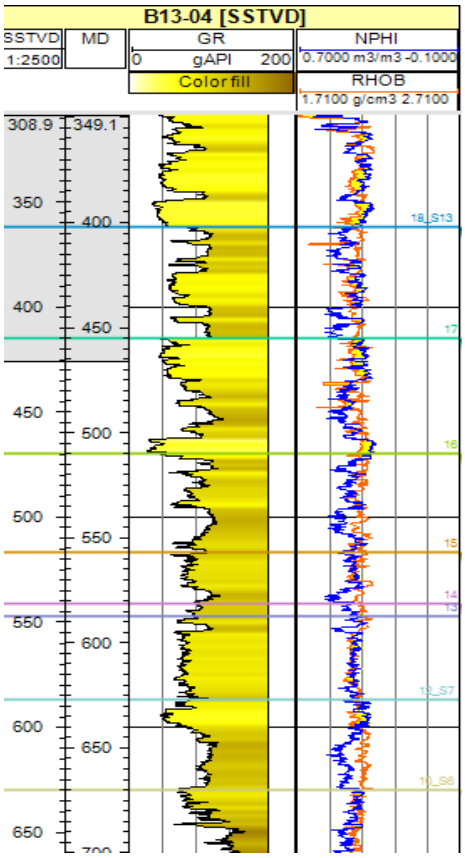

Figure 3-29. NPHI-RHOB well B13-04

MD (Seal)	**SSTVD (Seal)**	**Hydrocarbon column (m)** (Pressure data)	**Hydrocarbon column (m)** (Grain-size distribution)	**NPHI – RHOB Crossover (m)**
386 - 389	345.8 – 348.8	10	-	11
447.5 – 454.5	407.3 – 414.3	-	9	15
488 - 495	407.8 – 454.8	-	14	7
536 - 551	495.8 – 510.8	17	-	19 (not very clear)
649 - 669	608.8 – 628.8	-	15	20 (not very clear)

Table 3-10. Comparison between hydrocarbon columns calculated by pressure data and by grin-size distribution of the well A13-04

As is possible to see the figure and table above the pressure and grain-size measurements are very scarce and the cross-over between the NPHI and RHOB is very poorly in all the layers. In general there is an agreement between the data but the low quantity of the data is very hard to make comparison and give a proper interpretation to it.

3.7.5. Well B17-06

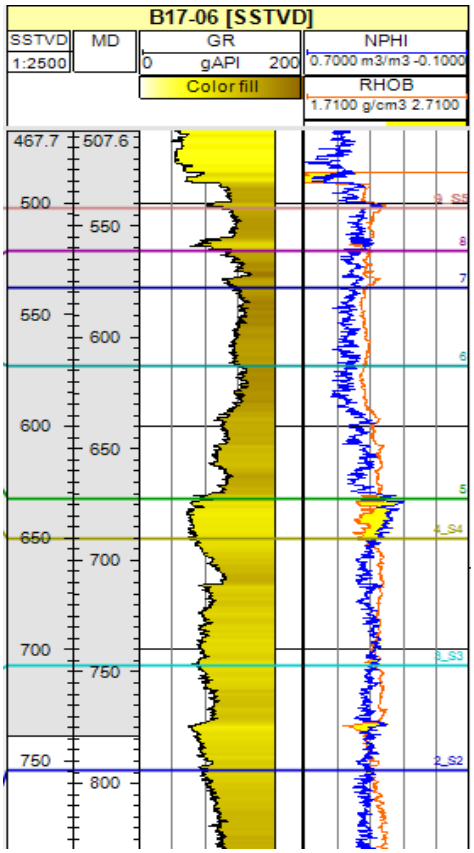

Figure 3-30. NPHI-RHOB well B17-06

MD (Seal)	**SSTVD (Seal)**	**Hydrocarbon column (m)** (Pressure data)	**Hydrocarbon column (m)** (Grain-size distribution)	**NPHI – RHOB Crossover (m)**
630 - 670	590 - 630	9	16	17 (+3)
759 - 772	719 - 732	-	6	4

Table 3-11.Comparison between hydrocarbon columns calculated by pressure data and by grin-size distribution of the well A17-06.

Even there are just a few measurements in this well there is a very good cross-over in a possible gas bearing layer. The data that correspond to its seal has a very good agreement with the sealing capacity calculated by the grain size distributions.

The hydrocarbon column calculated by the pressure data is giving value lesser than the others. One possible explanation is the fact that the pressure measurement was taken not exactly in the top of the hydrocarbon column for which could be underestimating the eight of the gas present in the layer.

CHAPTER IV.

CONCLUSIONS

The clay percentage is a fundamental parameter not only for the lithological characterization of the formations, is also for the calculation of permeability, porosity, pore throat radius and hence the sealing capacity. In very shallow environments the mudstone layers with high clay percentage are deposited with high porosity for which is decreased its sealing capacity.

Although some of the porosities values obtained by mudstone compaction are higher than the ones found in the literature for the formations present in the area of study, there is still a good correspondence between them. For this reason the assess of porosity from compaction is a good and reliable method for porosity calculation in mudstone layers.

There is a very good relation between the permeability values calculated and the pore throat radius for mudstone layers. As the pore throat radius also has a big influence in the calculation of the threshold capillary pressure , there was also found a good relation between it and the permeability. As a consequence having the values of absolute perpendicular bedding permeability of the formations allows to assess the pore throat radius and hence, knowing the characteristics of the fluid within the formation, its seal capacity.

The permeability values calculated for the mudstones layers was very low even being the porosity in some cases quite high. From this statement is possible to say that in the mudstones layers sampled if in some point is breached the capillary seal capacity, the low permeability will cause that there is still maintain a good value of hydrocarbon columns if there is a continuous migration or the gas through the formations.

The gas-bearing layers and the Mudstone layers with the best sealing properties are related with specific seismic stratigraphic units defined in the Dutch northern offshore. The glacial - interglacial environment in which the sediments had been deposited has also a direct influence in the seal capacity of the mudstones layers as its affects the grain-size distribution of the formations and as a consequence the porosity and pore throat radius. The seismic stratigraphic units with better seal capacity are in general de deeper ones for which if there is a similar clay percentage through all the formations, the higher hydrocarbons columns are going to be found in the deeper layers.

The agreement between the hydrocarbon column calculated by pressure data and the sealing capacity in the majority of the layers is quite good for which is possible to say that the grain-size distribution method applied in this study is a reliable tool for the top seal assessment calculation in a capillary leakage scenario. The principal constraint for the developed method is the lithology; was found that for a sand content grater that the 20 % accuracy of the relation between the permeability and pore throat is highly reduced and hence the reliability of this grain-size distribution method.

Although it is possible to measure capillary pressures in the laboratory to calculate the pore throat size and the heights of hydrocarbon column that may be present in the subsurface, the approach used in the study using grain size distributions to calculate the seal capacity has the advantage that there are many more grain-size analysis than capillary pressure measurements for which can be more widely applicable in hydrocarbon exploration.

RECOMMENDATIONS

- Develop a dynamic model of gas leakage in the mudstones layers sampled

- Compare the hydrocarbon column height calculated from this method with the structurally lowest points in the traps that can retain the gas (spill points)

BIBLIOGRAPHY

A.C, A., & Macquaker, H. (2011). Mudstone diversity: origin and implications for source, seal, and reservoir properties in petroleum systems. *AAPG Bulletin, Vol.95, no.12* , 2031 - 2059.

Aplin, A., & Larter, S. (2005). Fluid flow, pore pressure, wettability, and leakage in mudstone cap rocks. *Evaluating fault and cap rock seals: AAPG Hedberg Seriesno. 2* , 1-12.

Aplin, A., & Yang, Y. (2004). definition and practical application of mudstone porosity-effective stress relationship. *Petroleum Geoscience, Vol.10* , 153-162.

Barboza, S., Alway, R., Akpulat, T., Esch, W., Hicks, P., & Gerdes, M. (2009). Stochastic evaluation of fluvial to marginal marine sealing facies. *Marine and Petroleum goelogy 26* , 445 - 456.

Berg, R. (1975). Capillary pressure in stratigraphic traps. *The American Association of Petroleum Geologist Bulletin. Vol 59, No. 6* , 939 - 956.

Blott, S., & Pye, K. (2001). GRADISTAT: A GRAIN SIZE DISTRIBUTION AND STATISTICS. *earth surface processes and landforms, vol. 26* , 1237 - 1248.

Boult, P., Lanzilli, E., Michaelsen, B., McKirdy, D., & Ryan, M. (1998). A new model for the Hutton/Birikhead reservoir/ seal model couplet and the associated Birkhead-Hutton petroleum sustem. *Appea journal* , 724-744.

Brown, R. (2003). Soil Texture. *Fact Sheet SL-29* . Florida: Soil and Water Science Department, Florida Cooperative Extension Service, Institute.

Clayton, C., & Hay, S. (1994). Gas migration mechanisms from accumulation to surface . *Bulletin of the geological Society of Denmark, Vol.44* , 12-23.

Coal Geology. (n.d.). Retrieved July 31, 2012, from Coal Geology and Mining: Consulting Services: http://coalgeology.com/gamma-ray-geophysical-logging-in-coal-reserve-evaluation/56/

Concoran, D., & Doré, A. (2002). Top Seal assessment in exhumed basin settings - some insights from Atlantic Margin and borderland basins. *Hydrocarbon Seal Quantification* , 89-107.

Darby, D. (2002). Seal properties, overpressure and stress in the Taranaki and East Coast Basins, New Zealand. *New Zealand Petroleun Conference Proceedings* (pp. 1-10). New Zealand: Institute of Geological and Nuclear Sciences.

Donders, T., Guasti, E., Verreusesel, R., Munsterman, D., verweij, H., Ten Veen, J., et al. (n.d.). Explore Shallow Gas.

Grauls, D. (2011, Novermber 14). Seal or Leak Criteria. *Geopressures and Seals in Petroleum Exploration* .

Hermanrud, C., Nordgard, H., & Teige, G. (2005). Seal failure related to basin-scale processes. *Evaluating fault and cap rock seals: AAPG Hedberg Series, no.2* , 13-22.

HORIBA, S. (2000). A guidebook to particle size analysis. HORIBA Instruments, Inc.

Ingram, G., Urai, J., & Naylor, M. (1997). Sealing processes and top seal assessment. *Hydrocarbon seals: Importance for exploration and production, NPF Special Publication 7* , 165 - 174.

Konert, M., & Vandenberghe, J. (1997). Comparison of laser grain size analysis with pipette and sieve analysis: a solution for the understimation of the clay fraction. *Sedimentology, vol. 44* , 523 - 535.

Li, S., Dong, M., Li, Z., Huang, S., & Qing, H. (2005). Gas breakthrough pressure for hydrocarbon reservoir seal rocks: implications for the security of long-term CO2 storage in the Weyburn field. *Geofluids,5* , 326 - 334.

Moeys, J. (2012, March 8). The soil texture wizard: R functions for plotting, classifying, transforming and exploring soil texture data.

Nakayama, K., & Sato, D. (2002). Prediction of sealing capacity by the grain size method. *Hydrocarbon Seal Quantification* , 51 - 60.

Norgard, H., Hermanrud, C., & Gunn, T. (2005). Seal capacity estimation from subsurface pore pressures. *Basin Research, no.17* , 583-599.

Schroot, B., & Schüttenhelm, R. (2003). Expressions of shallow gas in the netherlands North Sea. *Netherlands Journal of Geosciences* , 91-105.

Shepard, F. (1954). Nomenclature based on sand-silt-clay ratios. *Journal of Sedimentary Petrology, Vol. 24* , 151 - 158.

Survey, U. D. (n.d.). *USGS, Science for a changing world*. Retrieved 07 31, 2012, from http://pubs.usgs.gov/of/2006/1195/htmldocs/nomenclature.htm

Sylta, O. (2005). On the dynamics of capillary gas trapping: implications for the charging and leakage of gas reservoirs. *6th Petroleum Geology Conference* (pp. 625-631). London : Geological Society.

Technology, M. M. (2011). *Thermophysical Properties of Fluid Systems*. Retrieved August 01, 2012, from NIST Chemistry WebBook: http://webbook.nist.gov/chemistry/fluid/

Van den Boogaard, M., & Hoetz, H. (2012). Shallow Gas Play in the Netherlands Takes Off. *74th EAGE Conference & Exhibition.* Copenhagen: EBN.

Verweij, J., Ten Veen, J., De Briun, G., Nelskampo, S., Donders, T., Kunakbayeva, G., et al. (2012). Shallow gas migration and trapping in the Cenozioc Eridanos Delta deposits, Dutch offshore. *74th EAGE Conference & Exibition .* Denmark: TNO.

Whittaker, A. (1991). *The on-line mud logging handbook.* Ohio: Aegis group.

Wong, E., De Lugt, I., Kuhlmann, G., & Overeem, I. (2007). Tertiary. In *Geology of the Netherlands* (pp. 151 - 171). Amsterdam: Royal netherlands academy of arts and sciences.